Visualization of Mad2 Dynamics at Kinetochores, along Spindle Fibers, and at Spindle Poles in Living Cells

B.J. Howell,* D.B. Hoffman,* G. Fang,‡ A.W. Murray,§ and E.D. Salmon*

*Department of Biology, CB#3280, University of North Carolina at Chapel Hill, Chapel Hill, North Carolina 27599; ‡Department of Biological Sciences, Stanford University, Stanford, California 94305-5020; and §Department of Physiology, University of California at San Francisco, San Francisco, California 94143-0444

Abstract. The spindle checkpoint prevents errors in chromosome segregation by inhibiting anaphase onset until all chromosomes have aligned at the spindle equator through attachment of their sister kinetochores to microtubules from opposite spindle poles. A key checkpoint component is the mitotic arrest–deficient protein 2 (Mad2), which localizes to unattached kinetochores and inhibits activation of the anaphase-promoting complex (APC) through an interaction with Cdc20. Recent studies have suggested a catalytic model for kinetochore function where unattached kinetochores provide sites for assembling and releasing Mad2–Cdc20 complexes, which sequester Cdc20 and prevent it from activating the APC. To test this model, we examined Mad2 dynamics in living PtK1 cells that were either injected with fluorescently labeled Alexa 488-XMad2 or transfected with GFP-hMAD2. Real-time, digital imaging revealed fluorescent Mad2 localized to unattached kinetochores, spindle poles, and spindle fibers depending on the stage of mitosis. FRAP measurements showed that Mad2 is a transient component of unattached kinetochores, as predicted by the catalytic model, with a $t_{1/2}$ of ~24–28 s. Cells entered anaphase ~10 min after Mad2 was no longer detectable on the kinetochores of the last chromosome to congress to the metaphase plate. Several observations indicate that Mad2 binding sites are translocated from kinetochores to spindle poles along microtubules. First, Mad2 that bound to sites on a kinetochore was dynamically stretched in both directions upon microtubule interactions, and Mad2 particles moved from kinetochores toward the poles. Second, spindle fiber and pole fluorescence disappeared upon Mad2 disappearance at the kinetochores. Third, ATP depletion resulted in microtubule-dependent depletion of Mad2 fluorescence at kinetochores and increased fluorescence at spindle poles. Finally, in normal cells, the half-life of Mad2 turnover at poles, 23 s, was similar to kinetochores. Thus, kinetochore-derived sites along spindle fibers and at spindle poles may also catalyze Mad2 inhibitory complex formation.

Key words: cell cycle • mitosis • spindle checkpoint • chromosome • microtubule

Introduction

The gain or loss of a single chromosome kills cells, contributes to tumor progression, and leads to birth defects. Therefore, to prevent aneuploidy, cells have evolved a surveillance mechanism, known as the spindle checkpoint, which regulates anaphase onset and prevents entry into anaphase until all chromosomes have become properly attached and aligned on the spindle. Continuing chromosome loss and gain is seen in most colorectal cancers (Lengauer et al., 1997) and probably many other types of cancer, and can result from mutational inactivation of a spindle checkpoint protein (Cahill et al., 1998).

Genetic screens in budding yeast have identified several components of the spindle checkpoint. These include the kinetochore proteins Mad1, 2, and 3 (Li and Murray, 1991), budding uninhibited by benzimidazole (Bub)[1] 1, 2, and 3 (Hoyt et al., 1991), and Mps1 (Hardwick et al., 1996; Weiss and Winey, 1996), which are required to delay cell cycle progression in response to spindle damage or to defects in kinetochore and centromere structure. Homo-

The online version of this article contains supplemental material.

Address correspondence to B.J. Howell, Department of Biology, CB#3280, University of North Carolina at Chapel Hill, Chapel Hill, NC 27599. Tel.: (919) 962-2354. Fax: (919) 962-1625. E-mail: bhowell@email.unc.edu

[1]*Abbreviations used in this paper:* APC, anaphase-promoting complex; Bub, budding uninhibited by benzimidazole; GFP, green fluorescent protein; hMad2, human Mad2; Mad2, mitotic arrest–deficient protein 2; XMad2, *Xenopus* Mad2.

logues of the mitotic arrest–deficient protein 2 (Mad2) and other checkpoint components have been identified recently in fission yeast and higher eukaryotes and shown to be highly conserved. For example, *Xenopus* Mad2 (XMad2) shares a 41 and 81% identity with the yeast (scMad2) and human (hMad2) homologues, respectively (Chen et al., 1996; Li and Benezra, 1996). Further studies have shown Mad2 to have important roles in the spindle checkpoint in these organisms (for review see Hardwick, 1998). For instance, in yeast and mice, the absence of Mad2 results in increased frequency of spontaneous chromosome loss (Li and Murray, 1991; Amon, 1998; Hardwick, 1998; Dobles et al., 2000), and in mammalian cells and cytoplasmic extracts, electroporation or microinjection of anti-Mad2 antibodies allows cells that have not aligned all of their chromosomes on the spindle to enter anaphase (Chen et al., 1996, 1998; Li and Benezra, 1996; Gorbsky et al., 1998; Waters et al., 1998; Canman et al., 2000). Furthermore, Mad2-null mouse cells do not arrest in response to spindle damage, show widespread chromosome missegregation, and undergo apoptosis during initiation of gastrulation (Dobles et al., 2000). Mad2 and several other checkpoint components have been shown to immunolocalize to kinetochores that lack bound microtubules or have only a small fraction of their microtubule binding sites occupied, and to disappear from kinetochores as they become fully occupied with kinetochore microtubules during chromosome alignment at the spindle equator in prometaphase (for reviews see Hardwick, 1998; Rieder and Salmon, 1998; Amon, 1999). Mad1 has been shown to be required for Mad2 localization to unattached kinetochores (Chen et al., 1998).

A variety of evidence suggests the defects that activate the spindle checkpoint occur at kinetochores (Rieder and Salmon, 1998). In 1995, Rieder et al. demonstrated that destruction of the last unattached kinetochore by laser ablation causes cells to enter anaphase. Furthermore, using micromanipulation of meiotic insect spermatocytes to move a chromosome far enough away from the metaphase plate to interfere with microtubule attachment inhibited anaphase onset (Li and Nicklas, 1995; Zhang and Nicklas, 1996). How does the cell know that a single kinetochore is improperly attached to the spindle?

Recent studies have identified a link between Mad2 and the cell cycle proteins that regulate anaphase onset (for review see Elledge, 1998). Initial studies in fission yeast identified a genetic interaction between Mad2 and the anaphase-promoting complex (APC; He et al., 1997). APC is involved in the ubiquitination and degradation of cyclin B1 (Holloway et al., 1993) and anaphase inhibitory proteins, such as Pds1/Cut2 (King et al., 1996), and its activation during mitosis requires an interaction with Cdc20 (Visitin et al., 1997; Fang et al., 1998; Hwang et al., 1998). Cdc20 has been shown to localize to kinetochores from late prophase to telophase, and partially to spindle microtubules and spindle poles (Kallio et al., 1998). Genetic analysis in fission and budding yeasts and biochemical experiments in frog egg extracts have shown that Cdc20 is the target that the spindle checkpoint inhibits; mutations in Cdc20 that block the binding of Mad2 destroy the checkpoint, and a tetrameric form of Mad2 binds Cdc20 and interferes with its ability to activate the APC in in vitro assays (Fang et al., 1998; Hwang et al., 1998; Kim et al., 1998). Therefore, the current model proposes that unattached kinetochores serve as catalytic sites for assembling Mad2–Cdc20 complexes, which sequester Cdc20 molecules that could otherwise bind to and activate the APC. It has been suggested that production of the inhibitory complex is halted when kinetochores on the last chromosome become attached to the spindle, allowing Cdc20 to dissociate from Mad2 and activate the APC (Kallio et al., 1998; Chen et al., 1998).

Immunofluorescence and biochemical studies have greatly enhanced our current understanding of the spindle checkpoint by localizing various checkpoint components to unattached kinetochores, and identifying the formation of checkpoint protein complexes (Chen et al., 1996, 1999; Taylor and McKeon, 1997; Fang et al., 1998; Gorbsky et al., 1998; Hwang et al., 1998; Kim et al., 1998; Waters et al., 1998). To examine Mad2 localization and dynamics in vivo and to test the transitory nature of Mad2 at unattached kinetochores, we microinjected living PtK1 cells with fluorescently labeled XMad2 or transfected the cells with green fluorescent protein (GFP)–hMAD2. Overall, by live cell analysis we found that fluorescent Mad2 is predominantly diffuse in the cytoplasm of PtK1 cells, localizes to unattached kinetochores during prophase, and depletes from kinetochores as they attach to the spindle. Furthermore, we observed cells entered anaphase ~10 min after depletion of Mad2 on the kinetochore of the last congressing chromosome. Using FRAP techniques, we demonstrated that Mad2 is a transient component of both kinetochores and spindle poles with an average $t_{1/2}$ of ~24–28 s. In addition, we found that treatment of cells with metabolic inhibitors resulted in a decreased turnover of Mad2 protein, whereas nocodazole treatment had little effect. Finally, we observed microtubule-dependent transport of Mad2 particles between kinetochores and spindle poles and found a subsequent loss of Mad2 protein at the spindle poles when it disappeared from proximal kinetochores. These observations indicate that a portion of Mad2 binding sites at kinetochores is translocated to spindle poles along the spindle fibers.

Materials and Methods

Cell Culture and Drug Treatment

PtK1 cells (American Type Culture Collection) were grown on coverslips and maintained in Ham's F12 medium, pH 7.2 (Sigma Chemical Co.) supplemented with 10% FBS, 100 U/ml penicillin, 0.1 mg/ml streptomycin, and 0.25 μg/ml amphotericin B in a 37°C, 5% CO_2 incubator. Before microinjection or filming, cells were incubated in dye-free L-15 medium, pH 7.2 (Sigma Chemical Co.), supplemented with 7 mM Hepes, 10% FBS, and antibiotics/antimycotic solution as described above. For experiments in which nocodazole was used, 10 mg/ml nocodazole in DMSO stock (Sigma Chemical Co.) was diluted into L-15 medium for a final concentration of 20 μg/ml.

Mad2 Protein Expression, Purification, and Fluorescent Labeling

Full-length XMAD2 tagged with six histidines at the NH_2 terminus was expressed in *Escherichia coli* using Qiaexpress vector pQE10 (QIAGEN) as previously described by Chen et al. (1996). Recombinant XMad2 protein was purified under nondenaturing conditions according to the manufacturer's instructions. Purified protein was dialyzed against PBS (140 mM

NaCl, 2.5 mM KCl, 10 mM Na_2HPO_4, and 1.5 mM KH_2PO_4, pH 7.8) overnight and spun at 30,000 rpm, 4°C, for 20 min in a Beckman tabletop ultracentrifuge to remove any protein precipitate. Purified protein was run on an SDS 12.5% polyacrylamide gel and visualized by silver stain.

The pH of 1 mg XMad2 protein was adjusted to pH 8.2–8.6 with 0.1 M $NaHCO_3$, and added to 0.1 mg of Alexa 488 succinimidyl ester reactive dye (Molecular Probes, Inc.). After gentle stirring for 30 min at 25°C, the reaction was stopped for another 30-min period by the addition of 0.05 M hydroxylamine, pH 8.5. Fluorescent XMad2 protein was separated from unincorporated dye by centrifugation through a Bio-Spin P6 column (Bio-Rad Laboratories) preequilibrated with injection buffer (IB: 10 mM Na_2HPO_4, pH 7.4, 100 mM KCl, and 1 mM $MgCl_2$). The eluted fluorescent XMad2 protein was collected and centrifuged at 30,000 rpm, 4°C, for 20 min to remove protein aggregates, and spectroscopy readings were taken at A_{280} nm and A_{490} nm to determine the protein concentration and labeling efficiency. The final dye-to-protein ratio was ~3:1. The Alexa 488-XMad2 (6–7-μM stock) was distributed in 20-μl aliquots, frozen in liquid nitrogen, and stored at −80°C.

XMad2 protein in PBS buffer was subjected to sedimentation velocity ultracentrifugation at 12,000 rpm at 20°C for 3–4 h in an AN60-Ti rotor in a Beckman Optima XLA analytical ultracentrifuge equipped with absorption optics. A two-sector cell was used; one cell was loaded with 450 μl of buffer, and the other with 350 μl of XMad2 protein. Absorption scans were taken every 2 min at 290 nm and the average molecular mass for the whole distribution was determined using XLA Origin software (Beckman).

Microinjection

Before microinjection, coverslips were mounted in modified Rose chambers (Rieder and Hard, 1990) lacking the top coverslip, and the chambers were filled with Hepes-buffered, L-15 medium to sustain the cells (described above). A circle was inscribed on the bottom coverslip using a diamond-tip scribing objective (Carl Zeiss, Inc.) and was used as a reference for relocating injected cells. Alexa 488-XMad2 protein was diluted into IB and injected into interphase and mitotic cells at 1.5 μM (needle concentration) on a Zeiss IM microscope equipped with phase optics and a 40×, 0.75 NA objective. The microinjection system is essentially as described in Waters et al. (1996). The stage temperature was maintained at 32–34°C using a Sage air curtain incubator. Immediately after injection, the chamber was sealed by adding a top coverslip and filled using a syringe and needle with fresh, dye-free, high glucose (4.5 g/l) L-15 medium supplemented with 0.3 U/ml of the oxygen-scavenging enzyme, Oxyrase (Oxyrase, Inc.).

GFP-hMad2 Transfection and Expression

The full-length coding sequence for hMAD2 was subcloned between the 5′ BamHI and XbaI 3′ sites of the pCS2-GFP mammalian expression vector (a gift from Dr. Robert Davis, Harvard Medical School, Cambridge, MA) so that the GFP fusion gene was at the NH_2-terminal end of hMAD2. PtK1 cells were subcultured on 22-mm coverslips in 10-mm plastic Petri dishes and were transfected using Effectene (QIAGEN). Additional control cultures were transfected with the plasmid pCS2-GFP, which codes for GFP without hMAD2. After a 6–12-h incubation, cells were rinsed with PBS to remove the transfection mixture, incubated in Ham's F12 medium (as described above), and viewed 48 h later using fluorescence and phase-contrast microscopy.

Immunofluorescence

For Mad2 immunofluorescence, cells were rinsed quickly with 60 mM Pipes, 25 mM Hepes, pH 6.9, 10 mM EGTA, 4 mM $MgSO_4$ (PHEM) and lysed with 0.5% Triton X-100/PHEM for 5 min at 37°C. After a quick rinse in PHEM, cells were fixed for 20 min in freshly prepared 4.0% formaldehyde/PHEM at 37°C. The following steps were all carried out at room temperature (25°C). Cells were rinsed three times for 5 min with PBS containing 0.05% Tween-20 (PBST) and subsequently blocked with 10% boiled normal donkey serum/PHEM (Jackson ImmunoResearch Laboratories) for 60 min in a humid chamber to prevent nonspecific antibody binding. Cells were incubated for 45 min in primary antibodies diluted 1:100 into 5% donkey serum. Affinity-purified rabbit anti–XMad2 antibodies were isolated as described previously (Waters et al., 1998). After four 5-min rinses in PBST, cells were incubated for 45 min in secondary donkey anti–rabbit antibodies conjugated to rhodamine red-X and diluted 1:100 (Jackson ImmunoResearch Laboratories).

For fixation studies after laser photobleaching, cells were immediately rinsed in PHEM, and fixed within 10–15 s of photobleaching in freshly prepared 1% paraformaldehyde/PHEM for 45 s at 37°C. Cells were lysed with 0.5% Triton X-100/PHEM for 5 min at 37°C and fixed for an additional 20 min in 4.0% formaldehyde/PHEM at 37°C. Cells were further processed for anti-Mad2 immunofluorescence essentially as described above.

Microscopy and Laser Photobleaching

For fluorescence and phase microscopy studies, cells were placed in modified Rose chambers containing dye-free, high glucose (4.5 g/l), L-15 medium supplemented with Oxyrase (as described above) and imaged on a Nikon TE300 inverted microscope equipped with a sensitive, Orca 1–cooled CCD camera (Hamamatsu Photonics). Images were obtained using a 100× 1.4 NA Plan Apo phase 3 objective, a 100-W mercury arc (attenuated to ~10%) fluorescent light source, and a Chroma Hy-Q FITC filter set. Photobleaching experiments were performed essentially as described by Maddox et al. (2000). In brief, a 488-nm line from an argon laser (Spectra-Physics) was selected through a band-pass filter and shuttered to control exposure. The laser was passed through a beam expander and focused as a spot conjugate with the field diaphragm to a diameter at half-maximal intensity of 0.8 μm at the specimen plane (Maddox et al., 2000). A typical experiment consisted of imaging fluorescently labeled Mad2 kinetochores before opening the laser shutter for 25 ms, and recording fluorescence recovery by time-lapse microscopy. The microscope was controlled by MetaMorph imaging software (Universal Imaging Corp.), and the images were collected at various time intervals depending on the experiment, ranging from 1 frame every 2 s to 1 frame every 60 s, with exposure times of 250 ms. Either single focal planes or a through-focus z-series stack consisting of three frames at 0.5-μm intervals were acquired at each time point, depending on experimental conditions. For temporal studies of anaphase onset, a through-focal series consisting of 0.3–0.4-μm steps was taken through the cell after the last chromosome congressed to the metaphase plate to ensure depletion of fluorescent Mad2 from all kinetochores.

Metabolic Inhibitor Treatment

For studies of Mad2 turnover in ATP-reduced cells, cells were injected with Alexa 488-XMad2, rinsed twice in saline G (140 mM NaCl, 5 mM KCl, 0.6 mM $MgSO_4{\cdot}7H_2O$, 0.1 mM $CaCl2{\cdot}2H_2O$, 1 mM $Na_2HPO_4{\cdot}7H_2O$, 1 mM KH_2PO_4, pH 7.3 supplemented with 4.5 g/L glucose) to remove culture medium, and were assembled in a sealed Rose chamber. The chamber was perfused with saline supplemented with 5 mM sodium azide (Sigma Chemical Co.), 1 mM 2-deoxyglucose (Sigma Chemical Co.), and 0.3 U/ml Oxyrase for 5 min. Injected cells were imaged before and after photobleaching of single kinetochores. Occasionally, cells were rinsed free of inhibitors, incubated with saline G plus Oxyrase, and used for further photobleaching and image analysis. Untreated control cells were imaged in saline G supplemented with Oxyrase.

For studies of Mad2 localization in ATP-reduced cells, PtK1 cells were microinjected with Alexa 488-XMad2 and assembled into Rose chambers as described above. Cells were placed in saline G and imaged for fluorescent XMad2, incubated with saline supplemented with 5 mM sodium azide, 1 mM 2-deoxyglucose, and 0.3 U/ml oxyrase for 30 min at 37°C, and then reimaged. After a 5–10-min washout of inhibitors with saline G, cells were imaged again for Mad2 fluorescence. For nocodazole studies, cells were incubated in 20 μM nocodazole for 20 min at 37°C before incubation with the ATP inhibitors. Note, 20 μM nocodazole was present throughout the entire experiment and cells were always maintained at 37°C.

Statistical Analysis of FRAP Data

MetaMorph software was used to measure integrated fluorescence intensities of kinetochores and spindle poles. In brief, a small circle slightly larger than the kinetochore was placed over the entire area of a kinetochore (or spindle pole) and the area (A_s) and integrated fluorescence intensity (F_S) for each time point were logged into an Excel spreadsheet. A circle slightly larger than the smaller circle was placed over the smaller circle and used to measure kinetochore (or spindle pole) fluorescence plus cytoplasmic background fluorescence. Measurements of the area (A_L) and integrated fluorescence intensity (F_L) of the large circle per time point were recorded into the spreadsheet, and the following formula was used to subtract background fluorescence (F_{BG}) and to obtain integrated fluorescence intensity readings minus background:

$$F_S - F_{BG} = F_S - \frac{(F_L - F_S) \times A_S}{(A_L - A_S)}. \quad (1)$$

Graphs of integrated fluorescence intensity minus background versus time were plotted in Excel. Mad2 half-life (turnover rate) was calculated essentially as described by Maddox et al. (2000). In brief, the first-order rate constant k was determined as previously described (Salmon and Wadsworth, 1986). The exponential function:

$$F_{inf} - F(t) = [F_{inf} - F(0)]e^{-kt} \quad (2)$$

describes fluorescence recovery of the kinetochore (or spindle pole) after laser illumination. F_{inf} is the intensity of the photobleached region after maximal recovery; $F(0)$ is the intensity of the same region at $t = 0$ (first time point after laser irradiation). The first-order rate constant k was derived from the slope of a best-fit line through graphs of $[\ln[F_{inf} - F(t)]$ versus time for photobleached regions. The half-life of fluorescence recovery was calculated by $t_{1/2} = \ln 2/k$ (equation 2). The percent fluorescence recovery (%R) was calculated from F_{inf}, $F(0)$ and the prebleached fluorescence: $100\%\ [F_{inf} - F(0)]/[F_- - F(0)]$, where F_- is the prebleach fluorescence measurement. The t test and analysis of variance (ANOVA) were performed using Microsoft Excel.

Quantitation of Injected Mad2 Protein in Cells and at Unattached Kinetochores

Pulled glass microneedle tips were filled with 6.2 μM of Alexa 488-XMad2 in 1 mg/ml BSA and placed on the stage of an inverted microscope (model TE300; Nikon). BSA was used to block absorption of fluorescent XMad2 to needle surfaces. The tip of the needle was suspended in immersion oil above the 100× oil objective and brought into focus. Fluorescent XMad2 images were taken using the same settings described above for the injected cells. Integrated Mad2 fluorescence intensities were measured within a 4×8–μm box along regions in the tip ~4–5 μm in diameter for several needle preparations. After background subtraction, the net integrated fluorescence intensity was used to calculate the fluorescence per micromolar per microliter XMad2 (F_N). This number was used to estimate the concentration and number of molecules of injected XMad2 in mitotic cells in the following way. First, we calculated the average volume of a mitotic PtK1 cell by measuring the diameter of trypsinized cells; the mean diameter (d) was 22 ± 2.5 μm, which yielded an average cell volume $(V) = 4/3\pi(d/2)^3 = 6pL$. To obtain estimates of the concentration and the number of injected XMad2 molecules in the cell, we integrated the Mad2 fluorescence throughout the cell boundary (F_T) in late prophase or early prometaphase when the cell was extended or flat. The concentration of injected XMad2 = $F_T/(F_N \times V)$. The total injected XMad2 per cell = the concentration of injected Mad2 × $V \times N_{AV}$, where N_{AV} is Avogadro's number (6.023×10^{23} molecules/mole).

Online Supplemental Material

Quicktime movies of the time-lapse fluorescent and phase Mad2 images accompanying Figs. 2 (Videos 1 and 2), 5 A (Video 3), 8 (Video 4, an additional example) and 9 (Video 5) are available at http://www.jcb.org/cgi/content/full/150/6/1233/DC1.

Results

Fluorescent Mad2 Protein Localizes to Unattached Kinetochores and Spindle Poles in Living PtK1 Cells

Interphase and mitotic PtK1 cells were injected with fluorescent XMad2 protein, and Mad2 localization and mitotic progression were observed using digital imaging fluorescence and phase-contrast microscopy. PtK1 cells were chosen as a model system because they are flat, typically contain 11 large chromosomes, and have been used extensively in studies of the spindle checkpoint (Rieder et al., 1994, 1995; Gorbsky et al., 1998; Waters et al., 1998, 1999). After microinjection into the cytoplasm, we found that fluorescent XMad2 was diffuse throughout the cytoplasm but concentrated in the nucleus of interphase (data not shown) and prophase cells (Fig. 1 A). Consistent with previous anti-Mad2 immunofluorescence studies in PtK1 cells and other tissue culture lines (Chen et al., 1996; Waters et al., 1998; Gorbsky et al., 1998), fluorescent XMad2 localized strongly to kinetochores in late prophase (Fig. 1 A) and early prometaphase (Fig. 1 B) cells and remained localized to kinetochores until their chromosomes achieved bipolar attachment to the spindle during late prometaphase and early metaphase (Fig. 1 C and Fig. 2 D). In addition, fluorescent XMad2 protein localized to the spindle poles during prometaphase and early metaphase (Fig. 1 C, arrowheads), and was frequently observed along spindle microtubules (Fig. 1 B; see Fig. 8). In contrast to previous fixed cell studies (Chen et al., 1996; Li and Benezra, 1996; Gorbsky et al., 1998; Waters et al., 1998), fluorescent XMad2 was not enhanced above background at either the nuclear envelope or prophase centrosomes in living PtK1 cells. Fluorescent XMad2 protein was not evident on kinetochores, spindle microtubules, or at the spindle poles during late metaphase, anaphase, and telophase (Fig. 1 D; also see Fig. 2, E and F).

Destruction of the spindle by the microtubule-depolymerizing agent nocodazole stimulates the spindle checkpoint and inhibits cell cycle progression. Chen et al. (1996) and Waters et al. (1998) showed immunolocalization of XMad2 to kinetochores in tissue culture cells after nocodazole treatment. Therefore, we examined the ability of our fluorescent XMad2 protein to localize to kinetochores upon nocodazole-induced depolymerization of spindle microtubules in living PtK1 cells. Cells were incubated in 20 μM nocodazole for 20 min and injected with Alexa 488-XMad2. Consistent with previous immunofluorescence studies (Waters et al., 1998), we found that XMad2 localized to kinetochores but not to spindle poles in nocodazole-treated PtK1 cells (data not shown). This observation was independent of the order in which cells were injected with fluorescent protein or treated with nocodazole, and suggests Alexa 488-XMad2 protein can localize to kinetochores in the absence of microtubules and upon nocodazole-induced reactivation of the spindle checkpoint. We also examined the localization patterns of Alexa 488-XMad2 protein in other cell lines (e.g., LLC-PK, HeLa, and newt lung epithelia) and found qualitatively similar localization patterns to those described above (data not shown). These cells, however, were not used for further experimentation since they are either smaller, rounder, or contain more chromosomes than PtK1 cells, making it more difficult to image fluorescent Mad2 localization dynamics in vivo.

To quantitatively estimate the amount of injected XMad2 protein present in the cell and at unattached kinetochores, fluorescent XMad2 images were taken of microneedle tips filled with known concentrations of Alexa 488-XMad2 protein. XMad2 fluorescence intensities were measured within a known area of the glass microneedle and compared with measurements taken within an injected cell (described in Materials and Methods). For injected prometaphase cells containing ~150 nM Alexa 488-XMad2 protein, the amount of fluorescent protein at an unattached kinetochore was ~0.15% of the total cellular fluorescent XMad2 protein, based on the ratio of integrated fluorescence at kinetochores to the total fluorescence in the cell (Fig. 1 B, large arrowhead). The total

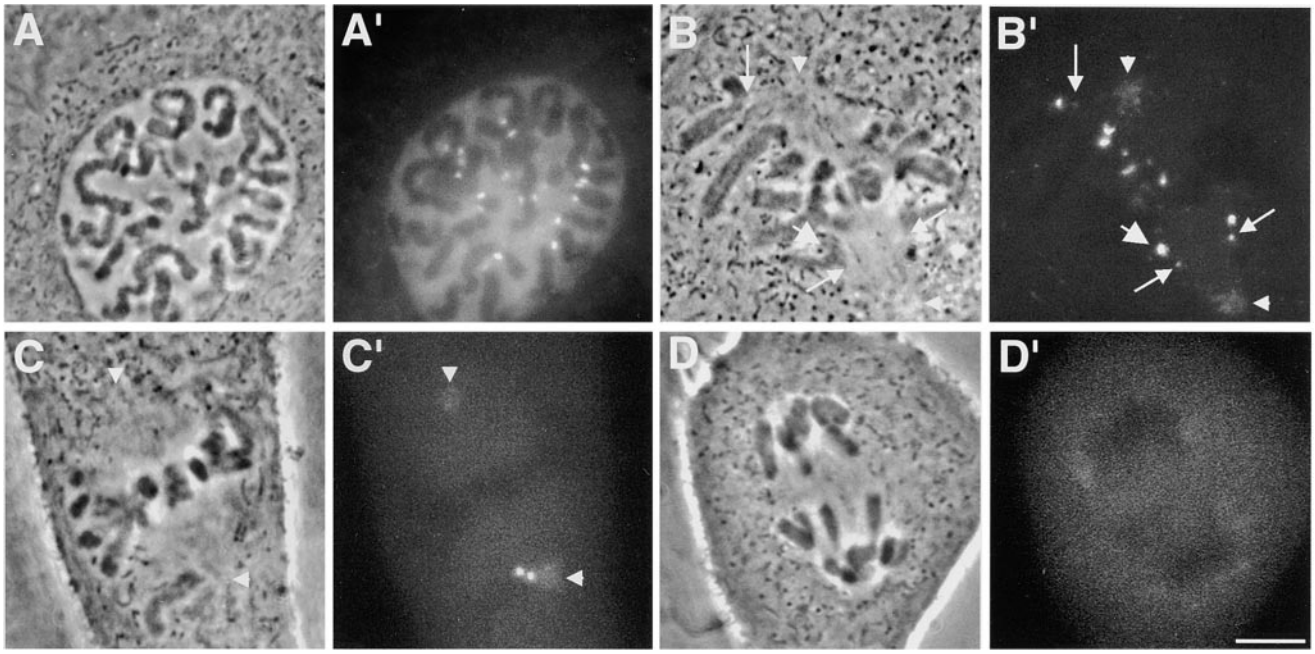

Figure 1. Fluorescent and phase-contrast images of living mitotic PtK1 cells injected with Alexa 488-XMad2. Fluorescent XMad2 is diffusely distributed in the cytoplasm and accumulates in the interphase nucleus. It localizes to unattached kinetochores in prophase (A) and early prometaphase (B, large arrowhead) and to the spindle poles in prometaphase (B and C, small arrowheads). Fluorescent XMad2 depletes from kinetochores upon their attachment to the spindle in prometaphase (B, small arrows) and is undetectable on aligned chromosomes (C). Fluorescent XMad2 is not present at kinetochores or spindle poles during anaphase and telophase. (D). Bar, 3 μm.

number of fluorescent XMad2 molecules in the cell was ~540,000 for an average cell volume of 6 pl (see Materials and Methods). Thus, the number of fluorescent XMad2 molecules bound to an unattached kinetochore at 0.15% of the total is ~810. We don't know the concentration of endogenous Mad2 in PtK1 cells, but believe it is likely near the 100 nM found in HeLa cells (Fang, G., unpublished observations). At 100 nM of endogenous Mad2 plus 150 nM of injected Alexa 488-Mad2 and a 6-pl cell volume, we estimate the total number of Mad2 molecules at a single unattached kinetochore to be ~1,300. At intracellular concentrations of injected Alexa 488-Mad2 above ~1,500 nM, the amount of Alexa 488-Mad2 at kinetochores appeared to saturate at ~1,500–2,000 molecules (data not shown).

Mitotic Progression Is Unaltered by the Microinjection of Fluorescent XMad2

To assess if the injection procedure or the presence of a low concentration of Alexa 488-XMad2 (~150 nM final) affected cell cycle progression in PtK1 cells, we microinjected early mitotic cells with fluorescent XMad2 protein and followed cell progression through mitosis using time-lapse fluorescence and phase-contrast microscopy. Previous studies showed that anaphase onset occurs in PtK1 cells ~23 min after the last monooriented chromosome biorients and begins congression to the metaphase plate (Rieder et al., 1994). In addition, cytokinesis is completed ~30 min after anaphase onset (Canman et al., 2000). We found injected cells progressed normally through mitosis and showed no abnormal delays in the metaphase–anaphase transition (Fig. 2 and Videos 1 and 2 [available at http://www.jcb.org/cgi/content/full/150/6/1233/DC1]). The completion of cytokinesis and entry into interphase also appeared normal in injected cells compared with noninjected cells and previous studies (data not shown; Rieder et al., 1994; Canman et al., 2000). Cells injected with similar amounts of unlabeled recombinant XMad2 protein also showed a normal mitotic progression (data not shown). Collectively, these studies suggest neither the injection procedure nor the presence of low concentrations of unlabeled or fluorescent XMad2 protein alters mitotic progression.

We believe our fluorescent XMad2 probe is functionally active based on the localization patterns described above and the additional activity assays described below. For example, analytical ultracentrifugation revealed that our purified recombinant XMad2 protein has an average molecular mass of 107.5 kD (Fig. 3 A), which is similar to the molecular mass of the Mad2 complex shown by Fang et al. (1998) to inhibit Cdc20 activation of the APC in in vitro assays. Second, we found microinjection of excess unlabeled or Alexa 488–labeled XMad2 protein (>750 nM final) into PtK1 cells causes a mitotic block (data not shown), which is consistent with similar injection experiments in *Xenopus* (Chen et al., 1998; Fang et al., 1998) and overexpression studies in yeast (He et al., 1997). Additionally, previous studies have shown microinjection of cells with anti-Mad2 antibodies induces premature anaphase onset (Gorbsky et al., 1998; Waters et al., 1998; Canman et al., 2000). Therefore, as a third test of the functional activ-

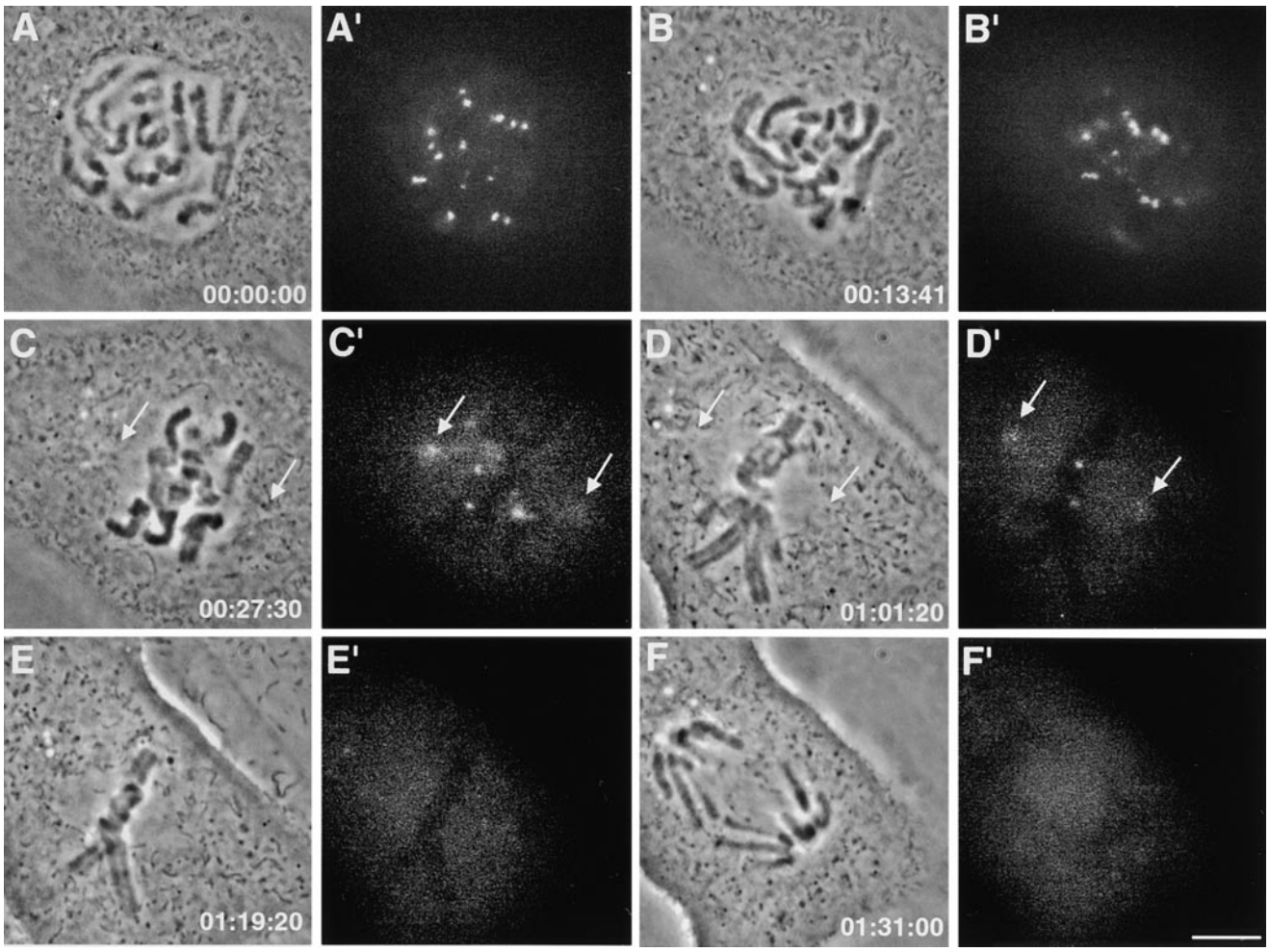

Figure 2. Time-lapse of fluorescent XMad2 protein in a living mitotic PtK1 cell. Fluorescent XMad2 localizes to kinetochores in prophase (A) and early prometaphase (B), and to spindle poles in prometaphase (C, arrows). Kinetochores leading chromosome congression to the metaphase plate often retain Mad2 localization (D) and polar localization persists (D, arrows). Fluorescent XMad2 diminishes at kinetochores in prometaphase (B and C) and at kinetochores and spindle poles in early metaphase (D). After Mad2 has been depleted from all kinetochores at late metaphase (E), the cells enter anaphase (F). Time is shown in hours:minutes:seconds. (See Videos 1 and 2 available online at http://www.jcb.org/cgi/content/full/150/6/1233/DC1). Bar, 3 μm.

ity of our labeled protein, we injected PtK1 cells with anti-Mad2 antibody to inactivate endogenous Mad2 protein (Fig. 3, B and C; Waters et al., 1998; Gorbsky et al., 1998; Canman et al., 2000), and subsequently injected the cells 3–4 min later with fluorescent XMad2 protein (Fig. 3 C). Real-time phase-contrast and fluorescence microscopy revealed our fluorescent XMad2 protein prevented premature anaphase onset in antibody-injected cells and that fluorescent XMad2 localized to kinetochores and spindle poles (Fig. 3 C). Finally, we compared the localization of our fluorescent XMad2 to that of GFP-hMad2 expressed in PtK1 cells and found similar localization patterns and behaviors (see Fig. 4; next paragraph).

GFP-hMad2 Shows Similar Localization Patterns in Living PtK1 Cells

As an alternative approach to using our recombinant Alexa 488-XMad2 probe, we expressed hMad2 protein fused to GFP in PtK1 cells and examined the localization pattern and dynamic behavior using real-time fluorescence and phase microscopy. Similar to our Alexa 488-XMad2 probe, GFP-hMad2 localized to unattached kinetochores in prophase (Fig. 4 A), and disappeared from kinetochores upon chromosome attachment to the spindle during late prometaphase/early metaphase (Fig. 4, B and C). GFP-hMad2 also localized to the spindle poles and along the spindle microtubules during prometaphase (Fig. 4, B and C), but was not evident at the kinetochores, spindle fibers, or spindle poles in anaphase (Fig. 4 D). Consistent with the Alexa 488-XMad2 studies, treatment of transfected mitotic PtK1 cells with 20 μM nocodazole resulted in GFP-hMad2 localization to the kinetochores but not to the spindle poles (data not shown). We found cells expressing low amounts of GFP-hMad2 or GFP alone progressed normally through mitosis (data not shown), but that high GFP-hMad2 expression often induced a mitotic block (data not shown). Overall, this localization pattern is consistent with previous reported immunofluorescent studies (Chen et al., 1996, 1998; Li and Benezra, 1996; Gorbsky et al., 1998; Waters et al., 1998) and with our fluorescent XMad2 probe and, therefore, indicates that GFP-

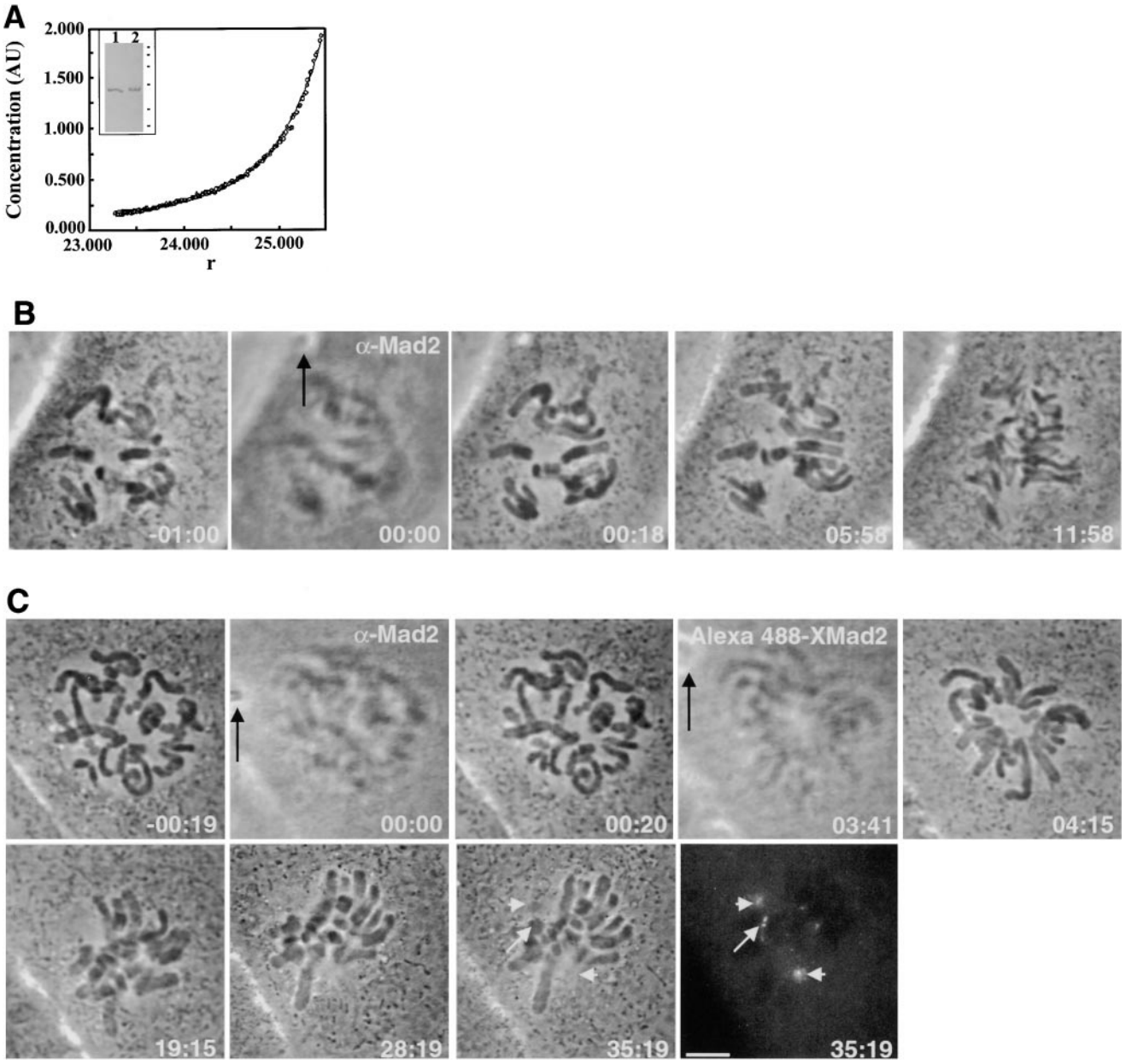

Figure 3. Characterization of purified XMad2 protein and analysis of its ability to inhibit premature anaphase onset in PtK1 cells injected with anti-Mad2 antibody. Unlabeled (A, inset lane 1) and Alexa 488–labeled XMad2 protein (A, inset lane 2) were run on a 12.5% SDS–polyacrylamide gel and purity was visualized by silver stain (A, inset). Sedimentation velocity ultracentrifugation was performed to determine the average molecular mass for the unlabeled XMad2. A graph of the concentration (absorbance units) as a function of rotor radius ($r = cm^2$) is shown in A. The shape of the sedimentation curve corresponds to an average molecular mass of 107.5 kD, as determined by the XLA Origin software (see Materials and Methods). B is a time-lapse sequence of premature anaphase onset in a PtK1 cell ~10 min after injection with anti-Mad2 antibody (black arrow). In C, a PtK1 cell is first injected with anti-Mad2 antibody (α-Mad2, black arrow), and then injected ~4 min later with fluorescent XMad2 (Alexa 488-XMad2). Time-lapse phase and fluorescent imaging shows that the cell does not enter anaphase prematurely and that the fluorescent XMad2 localizes to unattached kinetochores (small white arrow) and spindle poles (white arrowheads). M_r, markers are (top to bottom): 116, 66, 45, 31, 21.5, and 14 kD. Time is shown in minutes:seconds. Bar, 5 μm.

hMad2 and Alexa 488-XMad2 behave similar in living PtK1 cells.

FRAP Analysis Reveals Mad2 Protein Is a Transient Component of Kinetochores

The catalytic model of kinetochore function in the vertebrate spindle checkpoint proposes that unattached kinetochores serve as sites for assembling Mad2–Cdc20 complexes, which sequester Cdc20 and keep it from activating the APC (Chen et al., 1998; Kallio et al., 1998). To examine if Mad2 is a transient component of kinetochores, as predicted by this model, we used FRAP techniques to measure the turnover rate of fluorescent XMad2 protein

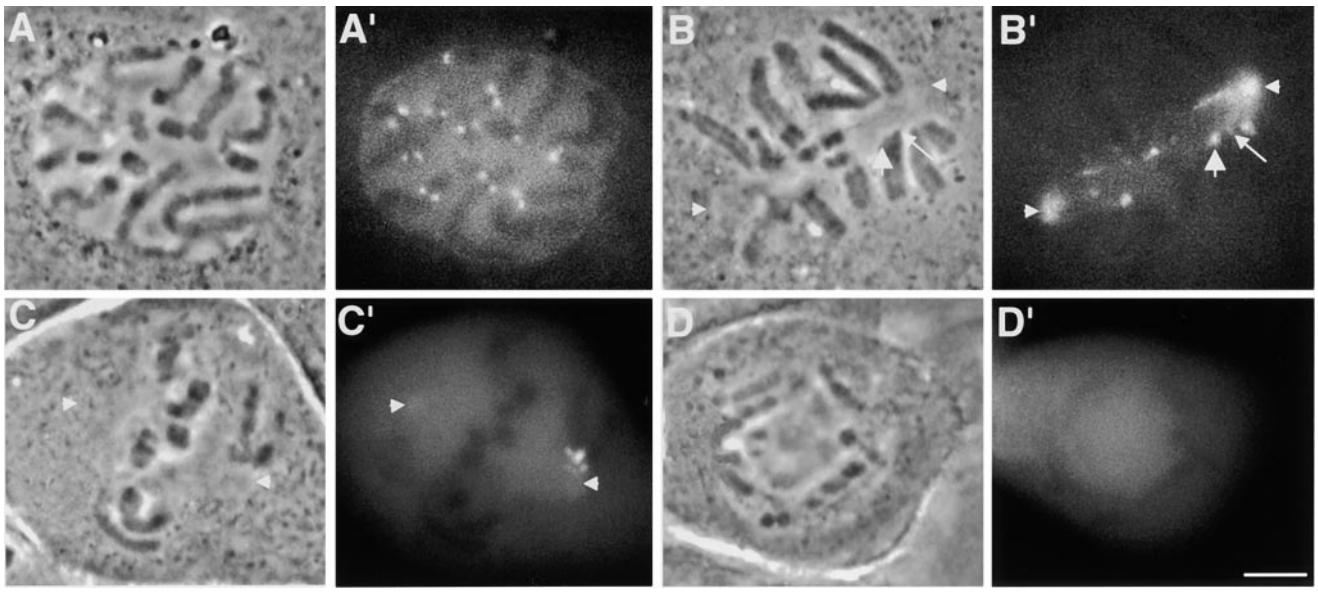

Figure 4. Fluorescent and phase images of GFP-hMad2 in living PtK1 cells. PtK1 cells were transfected with hGFP-MAD2 and observed for protein localization during mitosis. GFP-hMad2 accumulates in the nucleus and localizes to unattached kinetochores in prophase (A) and prometaphase (B, large arrowhead). During prometaphase, GFP-hMad2 is evident along some spindle fibers and at the spindle poles (B and C, small arrowheads). GFP-hMad2 fluorescence disappears from kinetochores as they became attached to the spindle in prometaphase (B, arrow) and aligned at the metaphase plate (C). GFP-hMad2 is not present at kinetochores, along spindle fibers, or at the spindle poles during anaphase (D) and telophase. Bar, 3 μm.

on unattached kinetochores. In brief, prophase and early prometaphase cells were microinjected with fluorescent XMad2 and unattached kinetochores were photobleached with a 25-ms exposure from a focused argon ion laser. The turnover rate of the fluorescent XMad2 protein at photobleached kinetochores was assessed from time-lapse images using quantitative fluorescence measurements.

The fluorescent time-lapse sequence from typical FRAP experiments and the corresponding graphs of fluorescence recovery can be seen in Fig. 5. In general, we found fluorescent XMad2 turnover occurred rapidly ($t_{1/2}$ = 26 s, n = 14) on prometaphase kinetochores and Mad2 fluorescence recovered an average of 84% of the initial bleached fluorescence (Fig. 5, A and A′, Table I, and Video 3 [available at http://www.jcb.org/cgi/content/full/150/6/1233/DC1]). This recovery percentage varied because of the attachment of some kinetochores to spindle microtubules during image acquisition. We compared fluorescent XMad2 turnover rates of prophase versus prometaphase kinetochores and found the means to be similar, as determined by a t test ($P < 0.01$; Table I). Thus, we combined the measurements and reported an overall mean turnover rate for prophase and prometaphase kinetochores ($t_{1/2}$ = 28 s, n = 19; Table I). Notably, although the means were not significantly different, we found there was a slight decrease in the mean turnover rate and a slight decrease in the mean percent fluorescence recovery of prophase kinetochores compared with prometaphase kinetochores (Table I). This observation could be due to differences in kinetochore structure, Mad2 complexes/binding affinities, or to the presence of spindle microtubules in prometaphase cells.

Next, we determined if the loss of spindle microtubules had any effect on the fluorescent XMad2 turnover rate in vivo. FRAP analysis was performed on fluorescent XMad2-labeled kinetochores in nocodazole-treated cells, and an example from a typical FRAP experiment can be seen in Fig. 5, B and B′. The turnover rate of fluorescent XMad2 protein at kinetochores in nocodazole-treated cells (32 s; n = 15; Table I) was not significantly different from the turnover rate observed in untreated cells ($P <$ 0.01; Table I), indicating a similar exchange rate with the cytoplasmic pool. Notably, however, we found the mean turnover rate in nocodazole-treated cells to be more similar to that observed for prophase kinetochores in untreated cells. In addition, the mean percent Mad2 fluorescence recovery in nocodazole-treated cells was similar to the mean percent fluorescence recovery in untreated prophase cells (~61% for nocodazole versus ~59% for prophase kinetochores; $P < 0.01$; Table I), but was significantly different from that of untreated prometaphase kinetochores (~84%; $P < 0.01$; Table I).

Since fluorescent XMad2 protein also localizes to spindle poles in prometaphase cells, we used FRAP techniques to test if fluorescent XMad2 is also a transient component of spindle poles. Using FRAP techniques, we observed a slightly faster turnover rate of Alexa 488-XMad2 protein at the spindle poles compared with that seen at the kinetochores (Fig. 5 C and Table I). For example, spindle poles had a mean Mad2 $t_{1/2}$ of 23 s and an average percent fluorescence recovery of ~95% (Fig. 5, C and C′, and Table I). However, using a t test, we found no significant difference ($P < 0.01$) in the mean turnover rates for the spindle poles versus prophase/prometaphase kinetochores. Interestingly, we observed a higher mean percent recovery at

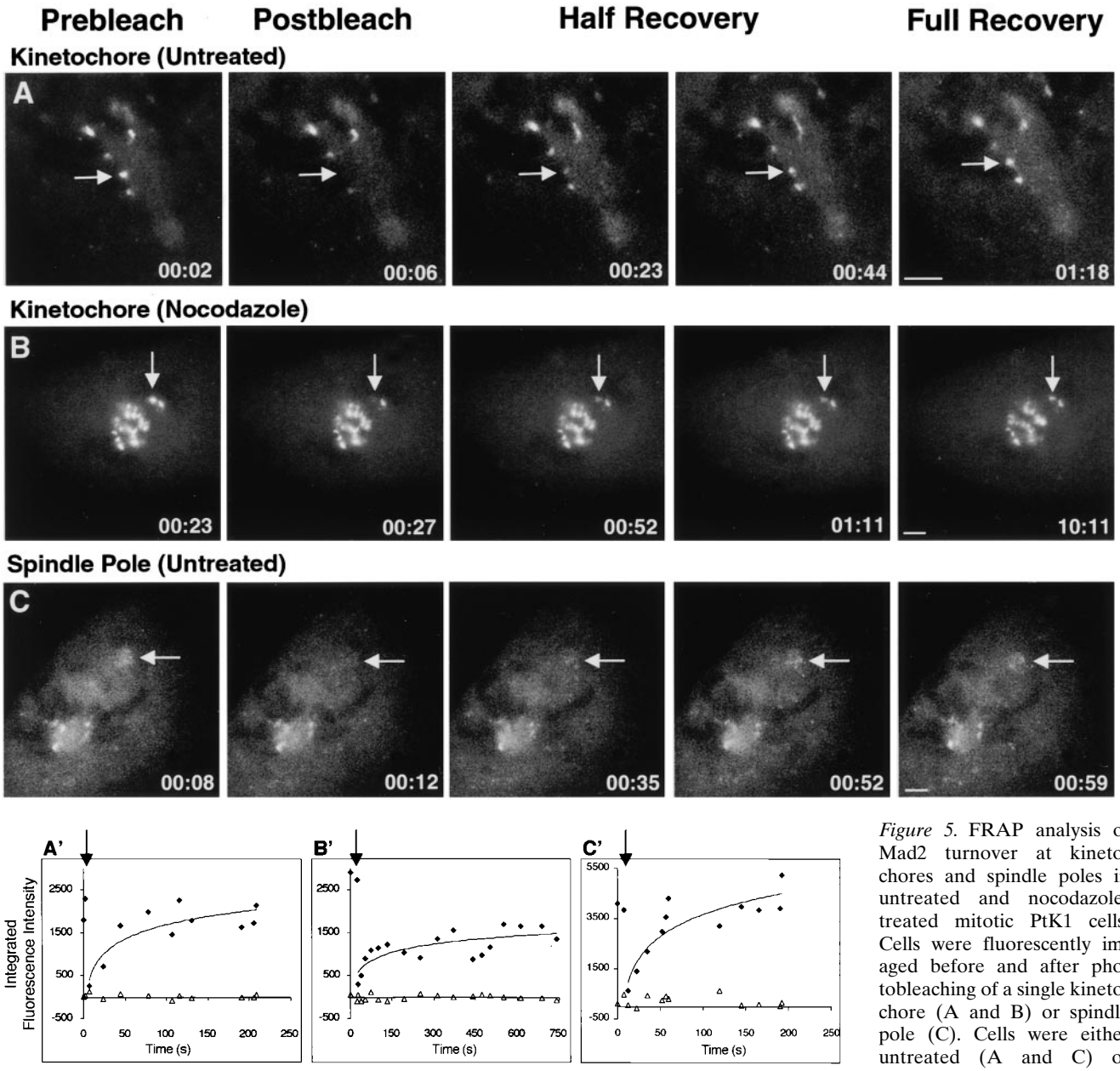

Figure 5. FRAP analysis of Mad2 turnover at kinetochores and spindle poles in untreated and nocodazole-treated mitotic PtK1 cells. Cells were fluorescently imaged before and after photobleaching of a single kinetochore (A and B) or spindle pole (C). Cells were either untreated (A and C) or treated with nocodazole for 20 min (B). The prephotobleach, postphotobleach, half recovery (two images), and full recovery time points are shown for each experiment. Arrows denote the photobleaching target. The time is shown in minutes:seconds. Also shown are the corresponding FRAP graphs of Mad2 turnover at bleached kinetochores (A′ and B′) and spindle poles (C′) in untreated (A′ and C′) and nocodazole-treated (B′) cells. A closed diamond is used to mark the photobleached kinetochores and spindle poles on the graph. Measurements of background fluorescence within the cytoplasm were also taken and are plotted on each graph (open triangles). Mad2 diffusion in the cytoplasm is rapid and the FRAP is too quick to record. Arrows denote time of photobleaching. (See Video 3 available online at http://www.jcb.org/cgi/content/full/150/6/1233/DC1). Bars, 3 μm.

spindle poles compared with the kinetochores, and often the recovery percentage of the poles exceeded the initial (prebleach) fluorescence intensity measurements.

Since Alexa 488-XMad2 and GFP-hMad2 proteins showed similar localization patterns in PtK1 cells, we extended our FRAP analysis of Mad2 turnover to cells transfected with GFP-hMAD2. In general, we found GFP-hMad2 turnover occurred rapidly ($t_{1/2}$ = 24 s, n = 12) on prometaphase kinetochores and recovered an average of 98% of the initial bleached fluorescence (Table I). FRAP analysis in nocodazole-treated GFP-hMad2 cells revealed an average $t_{1/2}$ of 32 s (n = 9) with a mean fluorescence recovery of 76% (Table I). Preliminary studies also suggest that GFP-hMad2 is a transient component of spindle poles with a mean $t_{1/2}$ of 21 s (n = 6) and an average fluorescence recovery of 90% (Table I). The consistency between the GFP-hMad2 and Alexa 488-XMad2 results suggests both probes are useful in characterizing Mad2 behavior in living

Table I. Summary of Mad2 FRAP Kinetics at Kinetochores and Spindle Poles in Living PtK1 Cells

Experimental conditions	k*	$t_{1/2}$*	Percent R*	n
	s^{-1}	s		
Alexa 488-XMad2				
Prophase kinetochores	0.020 ± 0.013	35 ± 23	59 ± 12	5
Prometaphase kinetochores	0.027 ± 0.010	26 ± 10	84 ± 23	14
Prophase and prometaphase kinetochores (summed)	0.025 ± 0.013	28 ± 15	78 ± 24	19
Nocodazole kinetochores	0.022 ± 0.009	32 ± 13	61 ± 17	15
Azide/deoxyglucose kinetochores	0.007 ± 0.003	102 ± 41	53 ± 19	6
Spindle poles	0.030 ± 0.014	23 ± 11	95 ± 31	16
GFP-hMad2				
Prometaphase kinetochores	0.028 ± 0.011	24 ± 9	98 ± 17	12
Nocodazole kinetochores	0.022 ± 0.010	32 ± 14	76 ± 10	9
Spindle poles	0.033 ± 0.011	21 ± 7	90 ± 24	6

*Determined by exponential regression analysis of recovery curves by plotting $\ln[F_{inf} - F(t)]$ versus time after photobleaching, as described in Materials and Methods. R, percent fluorescence recovery. Values are reported ± SD.

cells, and that the kinetic parameters listed in Table I reflect the dynamics of endogenous Mad2 at the kinetochores and spindle poles.

Photobleaching Does Not Destroy Mad2 at Kinetochores or Inhibit Kinetochore Function

The above conclusion is valid provided that photobleaching did not disrupt Mad2 binding to the kinetochore. To test this possibility, we combined fluorescence microscopy of living cells and immunofluorescence techniques to visualize fluorescent and nonfluorescent Mad2 protein on photobleached kinetochores. In brief, mitotic cells were microinjected with Alexa 488-XMad2 protein and then imaged before (Fig. 6, Prebleach) and after (Fig. 6, Postbleach) photobleaching of a single kinetochore. Within 10–15 s after photobleaching, cells were prefixed briefly to maintain the postbleached state of the kinetochore (Fig. 6, Alexa 488-XMad2) and further processed for immunofluorescent staining with anti-Mad2 antibodies (Fig. 6, α-Mad2). As seen in the fixed cell images, a small amount of fluorescent XMad2 protein is detectable on photobleached kinetochores (Fig. 6, Alexa 488-XMad2). This is not surprising, based on the turnover rate of fluorescent Mad2, and likely represents a partial turnover of fluorescent Mad2 protein on these kinetochores before the short prefixation period. In contrast, further immunofluorescence staining of the Mad2 protein using anti-Mad2 antibodies revealed a similar amount of Mad2 protein on the photobleached kinetochore compared with other unbleached kinetochores (Fig. 6, α-Mad2). This experiment shows that photobleached kinetochores retain normal levels of Mad2 protein, and further suggests that photobleaching does not significantly alter kinetochore structure or its ability to bind Mad2 protein.

To further assess possible deleterious effects of photobleaching on kinetochore function, we used fluorescence and phase-contrast microscopy to follow mitotic progression of cells in which Alexa 488-XMad2–labeled kinetochores had been previously bleached. We found that bleached kinetochores showed no abnormal delay in becoming attached to spindle microtubules and chromosomes always achieved proper alignment at the metaphase plate (data not shown). Furthermore, we observed normal transition periods between metaphase and anaphase onset, and proper segregation of sister chromatids whose kinetochores were previously photobleached (data not shown).

Mad2 Turnover Is ATP-dependent

The FRAP experiments described above demonstrate that Mad2 is a transient component of unattached kinetochores. Waters et al. (1999) have reported that Mad2 binding to kinetochores in lysed cell preparations requires kinetochore phosphorylation. To examine if Mad2 turnover requires metabolic energy, we performed FRAP analysis of labeled kinetochores in ATP-reduced mitotic cells. For these experiments, PtK1 cells were microinjected with Alexa 488-XMad2 protein and incubated for 5–7 min in 5 mM sodium azide and 1 mM 2-deoxyglucose (azide/deoxyglucose). Previous studies have used similar concentrations of these inhibitors to reduce cellular ATP levels by 70–90% in PtK1 cells after a treatment period of 5–15 min (DeBrabender et al., 1981; Bershadsky and Gelfand, 1983; Spurck et al., 1986a,b).

The results from FRAP experiments in azide/deoxyglucose-treated cells are shown in Table I. In general, we found Mad2 turnover to be significantly slower in azide/deoxyglucose-treated cells ($t_{1/2}$ = 102 s; $P < 0.01$; Table I) compared with untreated cells ($t_{1/2}$ = 28 s; Table I). Kinetochores in azide/deoxyglucose-treated cells had a mean percent fluorescence recovery of ~53% during the 5–7-min treatment period (Table I); FRAP analysis after longer treatments was not possible because of a depletion of Mad2 fluorescence at the kinetochores (see below). Interestingly, Mad2 fluorescence (see Fig. 10) and Mad2 turnover (data not shown) recovered to normal levels on these kinetochores after cells were rinsed free of metabolic inhibitors with saline G for 5–10 min, thus, illustrating the reversibility of azide/deoxyglucose treatment. Overall, this study suggests that Mad2 turnover at the unattached kinetochores is dependent on ATP.

Temporal Control of Fluorescent Mad2 Depletion on Lagging Chromosomes and Anaphase Onset

A previous study by Rieder et al. (1994) showed anaphase onset initiates in PtK1 cells ~23 ± 1 min after the last chromosome begins congression to the spindle equator. Furthermore, Gorbsky et al. (1998) demonstrated that Mad2 function is essential for maintaining the spindle checkpoint in PtK1 cells and that microinjection of cells with anti-Mad2 antibody causes premature anaphase onset within ~8 min. To examine the relationship between the loss of XMad2 at kinetochores and anaphase onset, we measured the interval between the loss of fluorescent Mad2 from kinetochores of the last chromosome to reach the spindle equator and the onset of anaphase. Late prophase cells were injected with Alexa 488-XMad2 and imaged using fluorescence and phase-contrast microscopy (Fig. 2). We found anaphase onset occurred 10.7 ± 1.2 min (n = 8) after depletion of fluorescent XMad2 on the kinetochores of the last congressing chromosome. Interestingly,

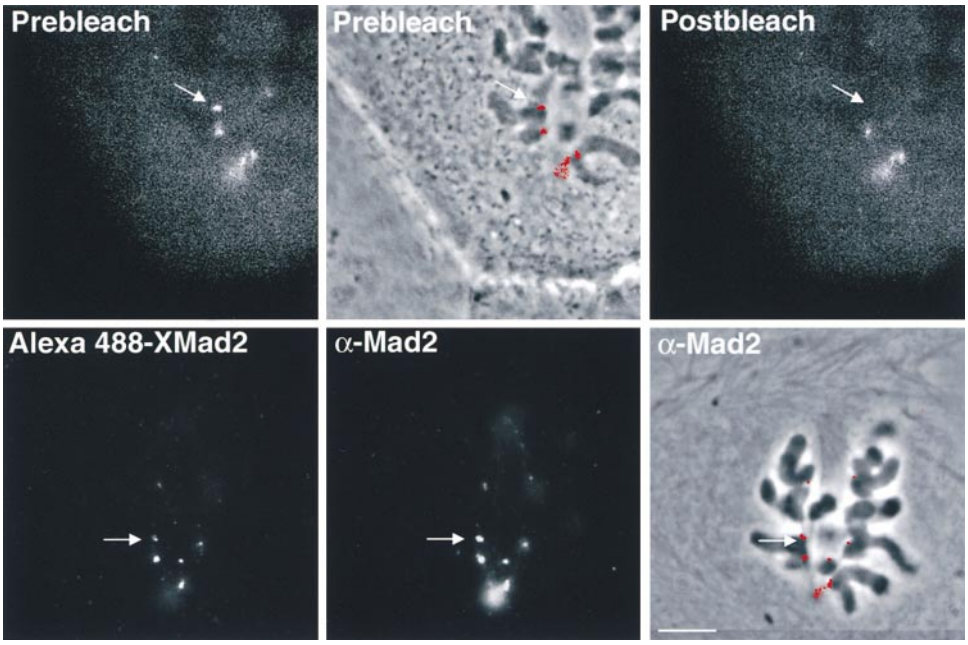

Figure 6. Photobleached kinetochores retain Mad2. PtK1 cells were injected with Alexa 488-XMad2 and imaged by fluorescence and phase-contrast microscopy immediately before (Prebleach) and after (Postbleach) photobleaching of a single kinetochore (arrows). Cells were quickly fixed (<15 s after photobleaching), lysed, and immunofluorescently processed for Mad2 using anti-Mad2 antibodies. Fixed cells show small amounts of exogenous Alexa 488-XMad2 fluorescence on photobleached kinetochores (Alexa 488-XMad2), however, anti-Mad2 staining revealed high concentrations of Mad2 protein on the photobleached kinetochore (α-Mad2). Bar, 3 μm.

10.7 min is similar to the time observed by Canman et al. (2000) between anti-Mad2 antibody injection and anaphase onset (11 ± 2 min, $n = 8$) in our PtK_1 cells. This suggests a temporal correlation between the loss of Mad2 protein on the last kinetochore and inactivation of the spindle checkpoint.

Visualization of Mad2 Dynamics at Kinetochores, Spindle Poles, and along Spindle Microtubules In Vivo

We further used our fluorescent Mad2 probes to visualize Mad2 and kinetochore structural dynamics in living cells as the kinetochores interacted with spindle microtubules during prometaphase. Using high resolution fluorescence and phase microscopy, we observed fluorescent Mad2 extensions emanating from kinetochores and stretching along microtubules in prometaphase and early metaphase cells (Fig. 7). These streaks varied in length, directionality, and duration, therefore, we have chosen to classify them into the following two categories: short streaks (<0.5 μm) that extended unidirectionally from the kinetochore and longer streaks (0.5–1.0 μm) extending in either one or both directions from a kinetochore along the spindle axis. The short unidirectional streaks (Fig. 7 A) often coincided with the direction of chromosome movement, and likely represented stretching of the kinetochore as it interacted with spindle microtubules. The longer streaks typically lasted longer than the shorter ones (Fig. 7, B and C). Notably, Mad2 stretching was never observed in prophase cells or cells treated with nocodazole (data not shown), indicating that extensions occur via a microtubule-dependent mechanism. Although we did not simultaneously visualize the interaction of individual microtubules with fluorescent Mad2-labeled kinetochores, we believe these streaks result from interactions between lateral microtubules and Mad2 complexes at the kinetochore. Streaks were also evident in PtK1 cells expressing GFP-hMad2 protein (data not shown).

In addition to the Mad2 extensions from kinetochores, fluorescent Mad2 protein was distributed along the spindle fibers between the kinetochore and the spindle pole (Figs. 8 and 4). This was observed in most cells and was especially frequent and evident on the spindle fibers between monooriented chromosomes and the spindle pole. On occasion, we also visualized the release of fluorescent Mad2 particles from kinetochores and transport of these particles towards the spindle poles (Fig. 8). In general, particles moved progressively in one direction from the kinetochore towards the spindle pole at a mean rate of 2–3 μm/min (Fig. 8 and Video 4). However, we did occasionally observe particles switching direction, pausing, or becoming displaced from the spindle microtubules (data not shown). An example of a particle being released from a kinetochore and transported to the spindle pole can be seen in Video 4 (available at http://www.jcb.org/cgi/content/full/150/6/1233/DC1).

When fluorescent Mad2 on a kinetochore disappeared, fluorescent Mad2 at the proximal pole also decreased and disappeared. This observation was most clearly seen in late prometaphase/early metaphase cells when only one or two chromosomes remained unattached and unaligned on the spindle (Fig. 9). In general, we observed a loss of Mad2 fluorescence on the kinetochores of the last congressing chromosome, and then a subsequent loss of Mad2 fluorescence at the proximal spindle pole (Fig. 9 and Video 5 [available at http://www.jcb.org/cgi/content/full/150/6/1233/DC1]). Fig. 9 C also clearly shows the localization of fluorescent Mad2 along spindle fibers between a labeled kinetochore and the proximal spindle pole. Notably, Mad2 fluorescence is not detected on other spindle microtubules/kinetochore fibers. These results collectively indicate that some Mad2 is transported to the spindle poles along spindle fibers. A loss of Mad2 at the kinetochore leads to a subsequent loss of Mad2 along spindle fibers and at the poles.

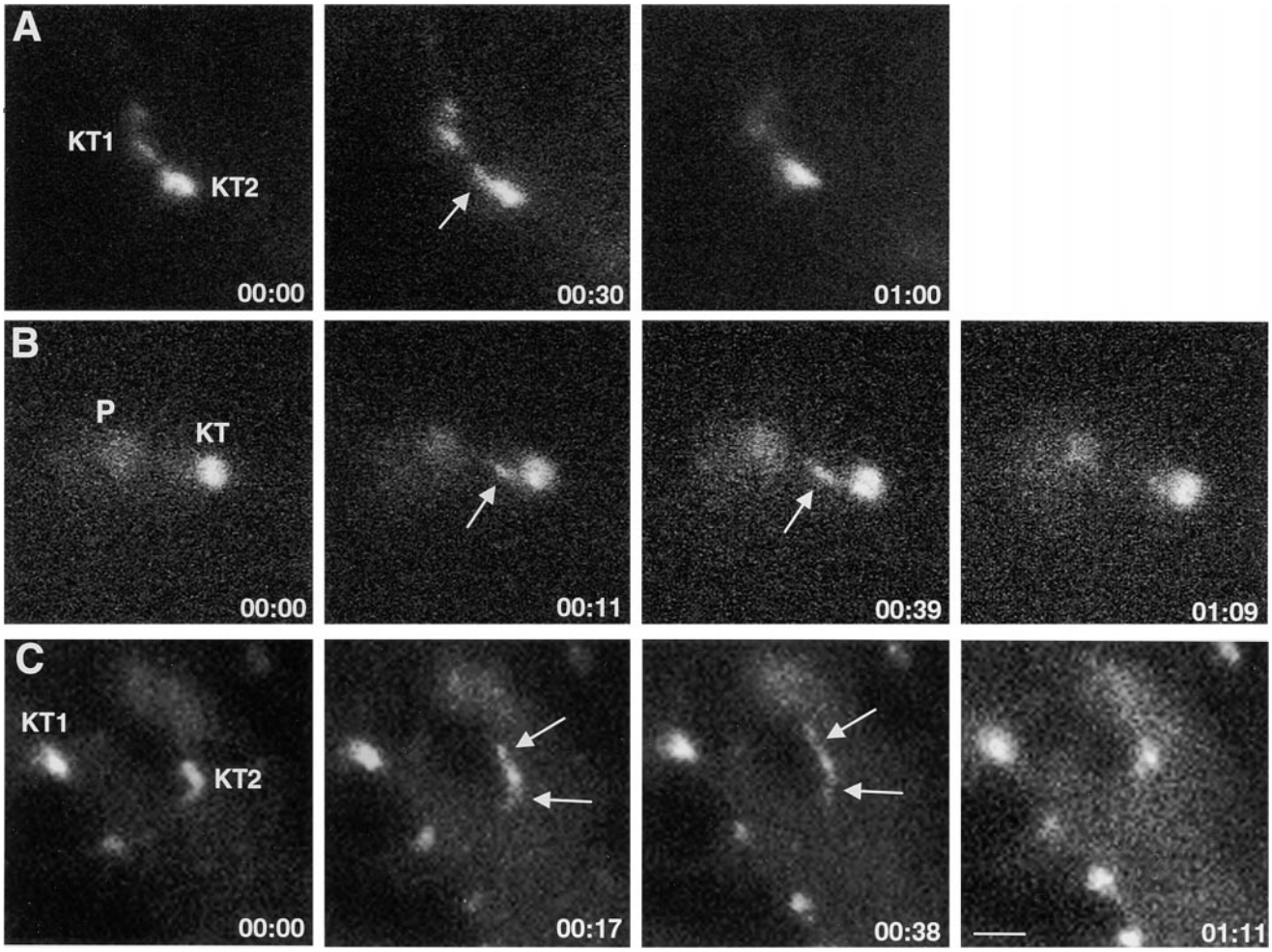

Figure 7. Fluorescent Mad2 is extended from kinetochores. Fluorescent XMad2 streaks extended from kinetochores in either one (A and B) or two (C) directions. KT denotes the location of the kinetochore, whereas P denotes the location of the spindle pole. Time is shown in minutes:seconds. Bar, 1 μm.

Evidence for microtubule-dependent transport of Mad2 complexes between kinetochores and the spindle poles was also obtained in our studies of the role of ATP in Mad2 localization. PtK1 cells were injected with Alexa 488-XMad2, treated with azide and 2-deoxyglucose for 30 min (a much longer period than the 5–7-min treatment used in the FRAP studies), and examined for fluorescent XMad2 localization. Before treatment with the ATP inhibitors, we found fluorescent XMad2 localized strongly to unattached kinetochores (Fig. 10 A) and to a lesser extent at the fibers and spindle poles in early prometaphase cells. Interestingly, Mad2 fluorescence became undetectable at the kinetochores and fibers and became highly concentrated at the spindle poles in prometaphase cells after the 30-min incubation with the ATP inhibitors (Fig. 10 B). After a 5–10-min washout period of the ATP inhibitors with saline G, we found that Mad2 fluorescence recovered to normal levels at the kinetochores and fibers and diminished at the spindle poles (Fig. 10 C). To test if the fluorescent Mad2 seen at the spindle poles is contributed from kinetochores versus the cytoplasm, we examined the effect of inhibitor treatment on metaphase cells since metaphase cells lack Mad2 at the kinetochores and the spindle poles (Fig. 2). We injected early metaphase cells with Alexa 488-Mad2 and imaged the cells before and after treatment with ATP inhibitors (Fig. 10, D and E). Notably, we found that fluorescent Mad2 protein remained undetectable at the kinetochores and spindle poles in ATP inhibitor–treated metaphase cells (Fig. 10 E). Identical results were also observed in fixed cell studies (data not shown) and suggest that Mad2 protein at kinetochores depletes from the kinetochores and accumulates at the spindle poles in cells with reduced ATP levels.

To test if this relocalization pattern from kinetochores to poles was dependent on spindle microtubules, we injected PtK1 cells with Alexa 488-XMad2, incubated them in nocodazole/saline G for 20 min, and imaged them for fluorescent XMad2. We found that fluorescent XMad2 localized to all the kinetochores, but was not evident at the spindle poles (Fig. 10 F). Cells were incubated in nocodazole and azide/deoxyglucose for 30 min and further imaged for fluorescent XMad2 localization. In contrast to the control cells, we were surprised to find the ATP inhibitors had no effect on Mad2 localization; i.e., fluorescent

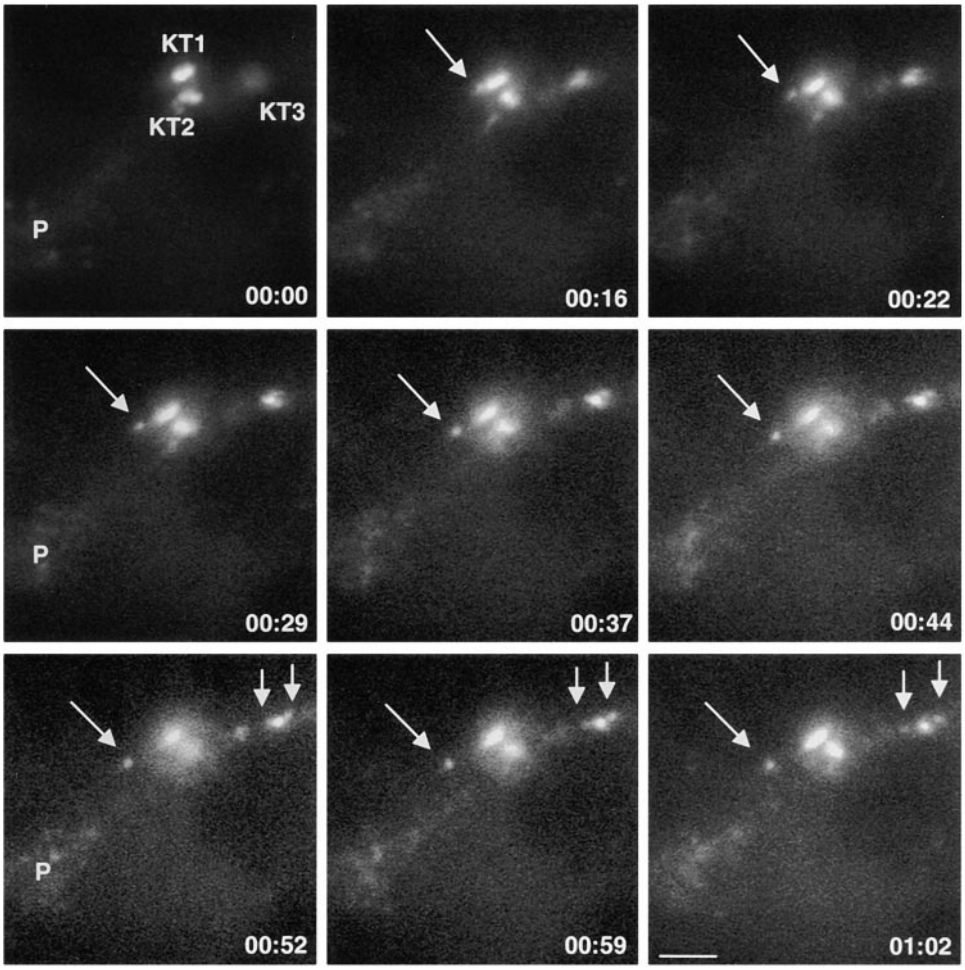

Figure 8. Release of fluorescent Mad2 particles from kinetochores. Fluorescent XMad2 particles were released from the kinetochore and transported towards the spindle pole via spindle microtubules. Arrows denote a release of fluorescent XMad2 particles. KT denotes the location of the kinetochore, whereas P denotes the location of the spindle pole. Time is shown in minutes:seconds. Bar, 2 μm. (See Video 4 available online at http://www.jcb.org/cgi/content/full/150/6/1233/DC1).

XMad2 was clearly evident on the kinetochores and not at the spindle poles (Fig. 10 G). Saline washout had no effect (Fig. 10 H). Therefore, this study indicates Mad2 relocalization from kinetochores to the spindle poles in azide/deoxyglucose-treated cells occurs through a microtubule-dependent translocation mechanism.

Discussion

Mad2 Localizes to Kinetochores, Spindle Poles, and Spindle Microtubules in Living PtK1 Cells

In this study, we examined the localization and dynamic behavior of Mad2 in living PtK1 cells using quantitative fluorescence and phase-contrast microscopy. After microinjection of Alexa 488-XMad2 or expression of GFP-hMad2 in PtK1 cells, we found Mad2 spread diffusely throughout the cytoplasm but accumulated rapidly in the nucleus of interphase and prophase cells, as previously described using immunofluorescence in *Xenopus* XTC tissue culture cells and mammalian HeLa and LLC-PK cells (Chen et al., 1996; Gorbsky et al., 1998; Li and Benezra, 1996). Fluorescent Mad2 also localized to unattached kinetochores in prophase, to the spindle fibers and poles during prometaphase, and then disappeared from the kinetochores upon attachment to the spindle during prometaphase and the spindle poles during late prometaphase. The localization of Mad2 to kinetochores in prophase may play a critical role in the spindle checkpoint. It suggests Mad2 inhibitory complexes form and begin to accumulate early in mitosis so as to prevent premature activation of the APC.

Our quantitative fluorescent XMad2 measurements indicate unattached prometaphase kinetochores contain between 1,000–2,000 binding sites for Mad2 protein. It is unclear which proteins form the Mad2 binding sites at kinetochores, along spindle fibers, and at the spindle poles. However, recent studies have shown that Mad1 is required for localization of Mad2 to kinetochores (Chen et al., 1998, 1999).

Our study of Mad2 dynamics in real-time revealed a loss of Mad2 fluorescence on the kinetochores of the last congressing chromosome with a subsequent loss of Mad2 fluorescence at the proximal spindle pole (Fig. 9). In addition, we also observed transportation of fluorescent Mad2 particles from the kinetochores to the spindle poles along spindle fibers, and found that the relocalization of fluorescent Mad2 to the spindle poles in azide/deoxyglucose-treated cells depended on spindle microtubules and the presence of Mad2 at kinetochores (Fig. 10). Collectively,

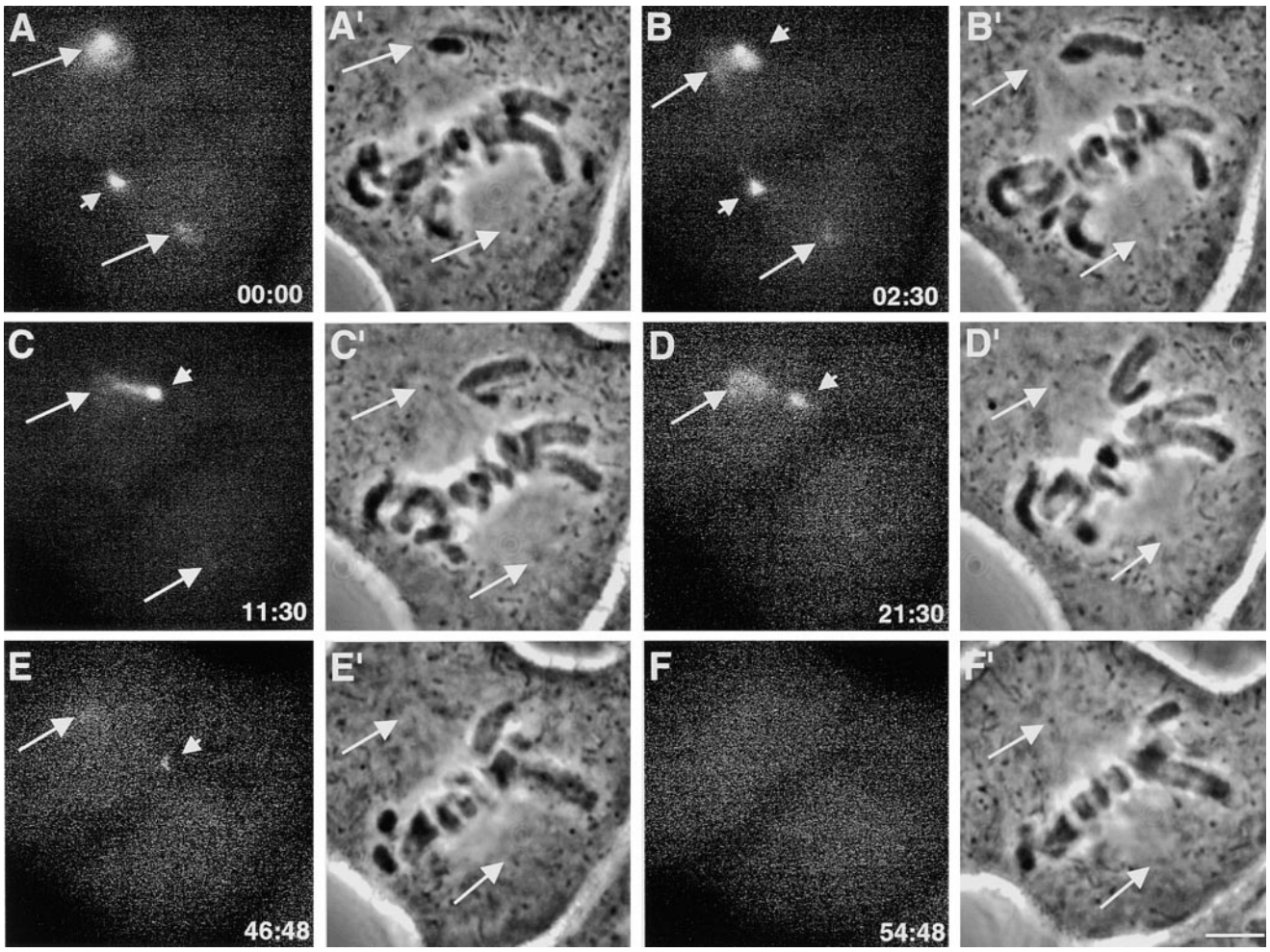

Figure 9. The loss of fluorescent XMad2 at spindle poles follows the loss of Mad2 localization to kinetochores. We observed the loss of fluorescent XMad2 at the kinetochore (small arrow) of a congressing chromosome and the subsequent loss of fluorescent XMad2 at the proximal spindle pole (B–E, large arrow). Interestingly, fluorescent XMad2 was only evident on the spindle pole proximal to the last monooriented chromosome (D–F). Time is shown in minutes:seconds. (See Video 5 available online at http://www.jcb.org/cgi/content/full/150/6/1233/DC1). Bar, 3 μm.

this indicates that spindle microtubules are involved in the translocation of some of the Mad2 binding sites at kinetochores to spindle poles.

Mad2 Is a Transient Component of Kinetochores and Spindle Poles

To test the transitory nature of Mad2 association at kinetochores, as proposed by current models, we used FRAP techniques to measure the turnover rate of fluorescent Mad2 protein on unattached and weakly attached kinetochores. We found that Mad2 turnover occurred rapidly on prophase and prometaphase kinetochores and displayed an average $t_{1/2}$ of 28 s for fluorescent XMad2; GFP-hMad2 had a similar $t_{1/2}$ of 24 s. Interestingly, we found no significant difference between the turnover rate of fluorescent Mad2 protein on kinetochores in prophase, prometaphase, and nocodazole-treated cells, indicating a similar exchange rate with the cytoplasmic pool. However, we did find that treating cells with azide and 2-deoxyglucose to reduce ATP levels resulted in a significant 3.5-fold decrease in the Mad2 turnover rate at the kinetochore (from ~28 s in untreated cells to ~102 s in azide/deoxyglucose-treated cells) before it became completely depleted from kinetochores. In general, this suggests that Mad2 is a transient component of unattached and weakly attached kinetochores and that Mad2 turnover is dependent on metabolic energy.

We found Mad2 had a similar, but slightly higher, turnover rate at the poles compared with kinetochores. Because of these similar FRAP rates, it is possible that Mad2 associated with the spindle microtubules and the spindle poles may also contribute to producing inhibitory complexes. If this is the case, then the inhibitory signal could be amplified beyond that produced by the kinetochore alone. It will be important to address in the future whether this dynamic turnover of Mad2 at kinetochores and spindle poles is necessary for checkpoint signaling.

Temporal Link between Kinetochore Mad2 Localization and Spindle Checkpoint Activity

Since the current model proposes checkpoint inactivation

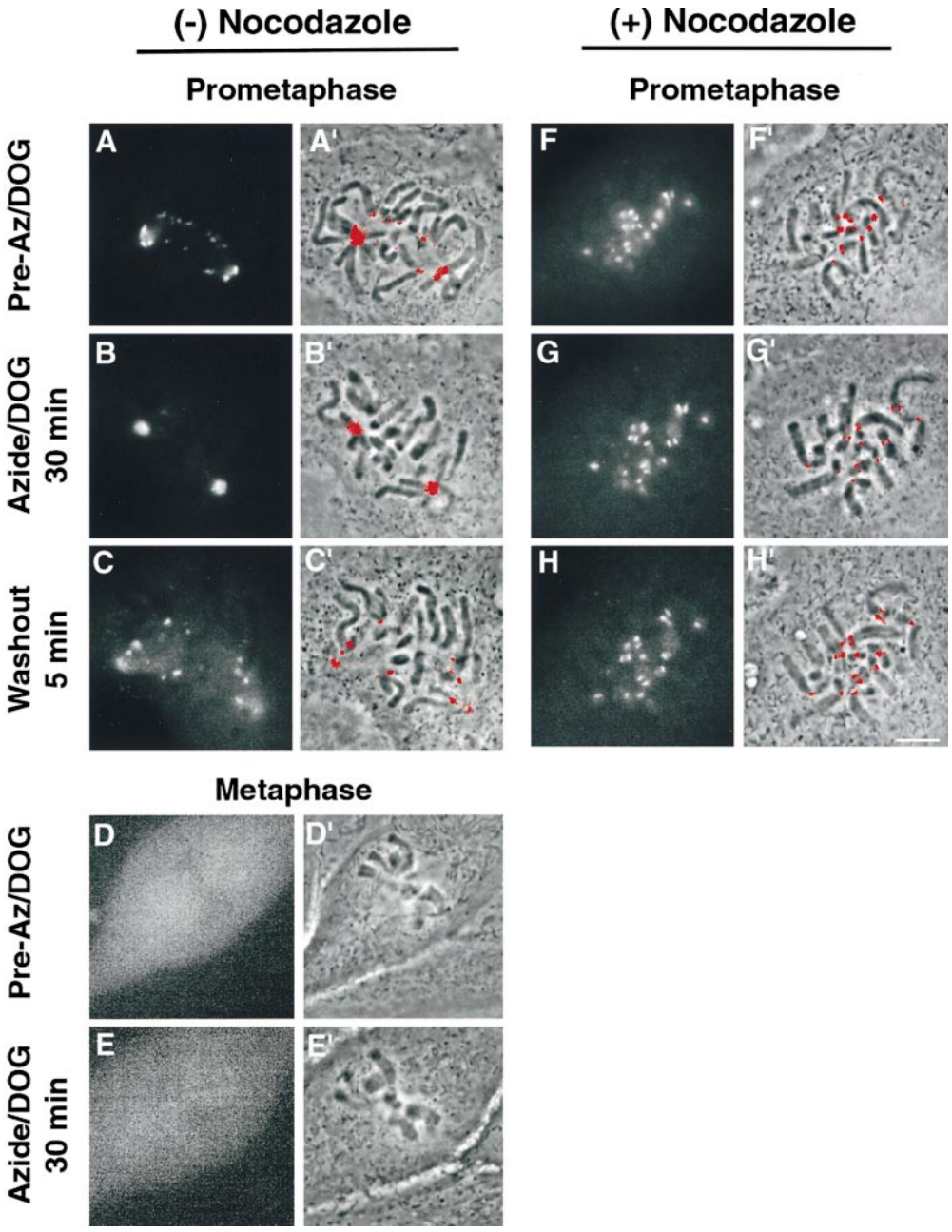

Figure 10. Mad2 fluorescence decreases at kinetochores and increases at spindle poles after ATP depletion in vivo if the spindle is present. Untreated (A–E) and nocodazole-treated (F–H) cells were injected with fluorescent XMad2 and imaged in saline with or without nocodazole (A, D, and F). Cells were incubated in medium containing 5 mM sodium azide and 1 mM 2-deoxy-glucose with or without nocodazole for 30 min, and reimaged for Mad2 localization (B, E, and G). Mad2 fluorescence concentrates strongly at the poles and is undetectable at kinetochores in prometaphase cells after 30 min treatment with inhibitors (B and B′), but remains in the cytoplasm in the metaphase cells (E and E′). After a saline rinse to wash out the inhibitors, Mad2 fluorescence quickly recovers on kinetochores and diminishes at spindle poles in prometaphase cells (C and C′). In contrast, however, Mad2 fluorescence remains at kinetochores and does not localize to spindle poles in nocodazole-treated cells after the 30-min incubation with the metabolic inhibitors (G and G′). Mad2 fluorescence in nocodazole-treated cells remains at the kinetochores after a brief washout of inhibitors with saline (H and H′). Bar, 5 μm.

occurs after depletion of Mad2 from all kinetochores, we used our fluorescent XMad2 probe to measure the time delay between the loss of Mad2 on the kinetochores of the last congressing chromosome and the onset of anaphase. Using time-lapse fluorescence microscopy, we found cells did not enter anaphase until all kinetochores had been depleted of fluorescent XMad2 during metaphase. Mad2 did not become completely depleted until the chromosome aligned at the metaphase plate, a position where all the microtubule binding sites become occupied (McEwen et al., 1997; for review see Rieder and Salmon, 1998). Overall, we found cells entered anaphase ~10 min after depletion of Mad2 on the last congressing chromosome. This finding correlates strongly with the data we and others have observed for the time delay between anti-Mad2 antibody injection and sister chromatid separation (Gorbsky et al., 1998; Canman et al., 2000). One interpretation of this 10-min delay is that the Mad2-Cdc20 inhibitory complex is very slow to dissociate (Fig. 11 A). However, this 10-min period is shorter than the 24-min period reported by Clute and Pines (1999) as the interval between the start of cyclin B degradation (APC activation) and anaphase onset. It will be important to examine in the same cell the quantitative relationship between the depletion of Mad2 at kinetochores and cyclin B degradation.

Proposed Model for Spindle Checkpoint Inactivation

Based on our observations, we suggest the following model for how a single kinetochore produces the wait-anaphase signal. We propose that microtubule attachment profoundly alters the structure of the kinetochore (see

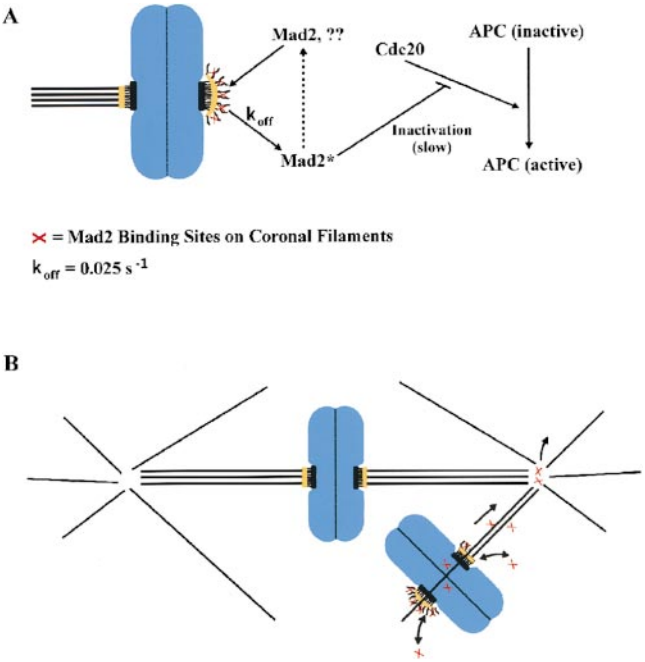

Figure 11. The proposed model for spindle checkpoint inactivation. Unattached kinetochores serve as catalytic sites for forming Mad2 inhibitory complexes (Mad2*), as suggested previously by Kallio et al. (1998) and Chen et al. (1998). Mad2 inhibitory complexes are released into the cytoplasm at a rate of 0.025 s^{-1}, where they prevent APC activation (A). Based on the 10-min delay between Mad2 depletion on the last chromosome and anaphase onset, inhibitory complexes are slowly inactivated (A). Interactions of kinetochores with spindle microtubules results in the depletion of coronal filaments containing Mad2 binding sites (x) from kinetochores and the translocation of some binding sites to the poles where they may also catalyze Mad2 inhibitory complexes before disassembly into the cytoplasm (B). Upon depletion of Mad2 binding sites from the kinetochores of the last congressing chromosome, inhibitory complex formation ceases at the kinetochores (and spindle poles), and the APC is activated.

also Rieder and Salmon, 1998). In the absence of microtubules, the kinetochore outer plate is a curved structure and is covered with coronal filaments (Fig. 11; Cassimeris et al., 1990; Thrower et al., 1996). Both of these features favor microtubule capture into sites in the outer plate. The filaments, which contain cytoplasmic dynein and CENP-E (for review see Rieder and Salmon, 1998), can capture microtubules by interacting with them laterally, whereas the curvature of the kinetochore plate allows it to make end-on interactions with microtubules over a wide range of angles. During the early stages of chromosome attachment to the spindle these features have the advantage that they allow kinetochores over a very wide range of orientations to capture microtubules that emanate from the spindle poles. But the very features that increase the probability of chromosome capture can also lead to problems in chromosome alignment, since a wide capture angle could allow one kinetochore to bind microtubules from both poles. We propose that this misalignment does not occur because kinetochores respond to microtubule interactions and attachment by losing their coronal filaments and changing the surface of the kinetochore to a small disk. A loss of the coronal filaments prevents interactions with the sides of microtubules and the disk-like kinetochore outer plate can only interact with microtubule ends over a narrow angular range, thus, preventing it from attaching to two spindle poles at the same time. These changes could be mechanically induced by the interactions with microtubules: minus end–directed motors on the coronal filaments would tear them out of the kinetochore and move them to the spindle poles, whereas the parallel orientation of microtubules from one pole would gradually force all the microtubule attachment sites to face towards that pole.

The behavior of Mad2 is most simply explained by proposing that coronal filaments and Mad2 binding sites are assembled at the kinetochore outer plate domain and can be transported by microtubules to the poles where they eventually disassemble (Fig. 11). The Mad2 binding sites convert Mad2 from an inert form to one that can bind to and inhibit Cdc20 (Fig. 11). Mad2 can leave the kinetochore in two ways: (1) by removal of the coronal filaments from the kinetochore, (2) or by the release of Mad2 from binding sites on the coronal filaments that remains attached to the kinetochore. The loss of the budding yeast Bub1 and Bub3 proteins makes cells very sick, whereas the loss of Mad1 or Mad2 has little effect in cells whose spindles are normal, even though *bub* and *mad* mutations appear to be equally defective in the spindle checkpoint (Roberts et al., 1994; for review see Hardwick, 1998). This observation encourages the speculation that Bub1 and Bub3 are the structural core of the coronal filaments, which are needed both to promote rapid microtubule capture and for the function of the spindle checkpoint. Allowing a polymeric filament that has multiple copies of the checkpoint proteins to generate the active signaling molecules has the advantage that a single unattached kinetochore (and secondarily at the spindle poles) can generate thousands of inhibitory complexes needed to inhibit most of the APC in the cell. Thus, upon depletion of Mad2 binding sites from the kinetochore of the last congressing chromosome, inhibitory complex formation ceases at the kinetochores (and subsequently at the spindle poles), and Cdc20 acquires the ability to activate the APC.

We would like to thank Dr. Rey-Huei Chen (Cornell University, Ithaca, NY) for providing the XMad2 clone and for advice on protein purification. Thanks to Dr. Bruce Nicklas (Duke University, Durham, NC) and to members of the Salmon and Bloom labs (University of North Carolina, Chapel Hill, NC) for a critical reading of this manuscript. Special thanks to Julie Canman (University of North Carolina, Chapel Hill, NC) for help with anti-Mad2 antibody injection in PtK1 cells.

This work was supported by a National Institutes of Health grant (NIHGMS No. 24364) to E.D. Salmon. Work in G. Fang's lab is supported by a Career Award from Burroughs Wellcome Fund, the Terman Fellowship from Stanford University, and a research grant from the Concern Foundation. Work in A.W. Murray's lab is supported by NIH and the Human Frontiers in Science Program.

Submitted: 24 March 2000
Revised: 3 August 2000
Accepted: 7 August 2000

References

Amon, A. 1999. The spindle checkpoint. *Curr. Opin. Gen. Dev.* 9:69–75.

Bershadsky, A.D., and V.I. Gelfand. 1983. Role of ATP in the regulation of the stability of cytoskeletal structures. *Cell Biol. Int. Rep.* 5:173–187.

Cahill, D.P., C. Lengauer, J. Yu, G.J. Riggens, J.K.V. Wilson, S.D. Markowitz, K.W. Kinzler, and B. Volgelstein. 1998. Mutations of mitotic checkpoint genes in human cancers. *Nature*. 392:300–303.

Canman, J.C., D.B. Hoffman, and E.D. Salmon. 2000. The role of pre-and post-anaphase microtubules in the cytokinesis phase of the cell cycle. *Curr. Biol*. 10:611–614.

Cassimeris, L., C.L. Rieder, G. Rupp, and E.D. Salmon. 1990. Stability of microtubule attachment to metaphase kinetochores in PtK1 cells. *J. Cell Sci*. 96:9–15.

Chen, R.-H., J.C. Waters, E.D. Salmon, and A.W. Murray. 1996. Association of spindle assembly checkpoint component Xmad2 with unattached kinetochores. *Scienc*e. 274:242–246.

Chen, R.-H., A. Shevchenko, M. Mann, and A.W. Murray. 1998. Spindle checkpoint protein Xmad1 recruits Xmad2 to unattached kinetochores. *J. Cell Biol*. 142:283–295.

Chen R.-H., D.M. Brady, D. Smith, A.W. Murray, and K.G. Hardwick. 1999. The spindle checkpoint of budding yeast depends on a tight complex between the Mad1 and Mad2 proteins. *Mol. Biol. Cell*. 10:2607–2618.

Clute, P., and J. Pines. 1999. Temporal and spatial control of cyclin B1 destruction in metaphase. *Nat. Cell Biol*. 1:82–87.

DeBrabender, M., G. Guens, R. Nuydens, R. Willebrords, and J. DeMey. 1981. Microtubule assembly in living cells after release from nocodazole block: the effects of metabolic inhibitors, taxol, and pH. *Cell Biol. Int. Rep*. 5:913–920.

Dobles, M., V. Liberal, M.L. Scott, R. Benezra, and P.K. Sorger. 2000. Chromosome missegregation and apoptosis in mice lacking the mitotic checkpoint protein Mad2. *Cell*. 101:635–645.

Elledge, S.J. 1998. Mitotic arrest: Mad2 prevents sleepy from waking up the APC. *Science*. 279:999–1000.

Fang, G., H. Yu, and M.W. Kirschner. 1998. The checkpoint protein Mad2 and the mitotic regulator CDC20 form a ternary complex with the anaphase-promoting complex to control anaphase initiation. *Genes Dev*. 12:1871–1883.

Gorbsky, G.J., R.-H. Chen, and A.W. Murray. 1998. Microinjection of antibody to Mad2 protein into mammalian cells in mitosis induces premature anaphase. *J. Cell Biol*. 141:1193–1205.

Hardwick, K.G. 1998. The spindle checkpoint. *Trends in Gen*. 14:1–4.

Hardwick, K.G., E. Weiss, F.C. Luca, M. Winey, and A.W. Murray. 1996. Activation of the budding yeast spindle assembly checkpoint without mitotic spindle disruption. *Science*. 273:953–956.

He, X., T.E. Patterson, and S. Sazer. 1997. The *Schizosaccharomyces pombe* spindle checkpoint protein Mad2p blocks anaphase and genetically interacts with the anaphase-promoting complex. *Proc. Natl. Acad. Sci. USA*. 94:7965–7970.

Holloway, S.L., M. Glotzer, R.W. King, and A.W. Murray. 1993. Anaphase is initiated by proteolysis rather than by the inactivation of MPF. *Cell*. 73: 1393–1402.

Hoyt, M.A., L. Trotis, and B.T. Roberts. 1991. *S. cerevisiae* genes required for cell cycle arrest in response to loss of microtubule function. *Cell*. 66:507–517.

Hwang, L.H., L.F. Lau, D.L. Smith, C.A. Mistrot, K.G. Hardwick, E.S. Hwang, A. Amon, and A.W. Murray. 1998. Budding yeast Cdc20: a target of the spindle checkpoint. *Science*. 279:1041–1044.

Kallio, M., J. Weinstein, J.R. Daum, D.J. Burke, and G.J. Gorbsky. 1998. Mammalian p55CDC mediates the association of the spindle checkpoint protein Mad2 with the cyclosome/anaphase promoting complex and is involved in the regulation of anaphase onset and late mitotic events. *J. Cell Biol*. 141: 1393–1406.

Kim, S.H., D. Lin, S. Matsumoto, A. Kitazono, and T. Matsumoto. 1998. Fission yeast Slp1: an effector of the Mad2-dependent spindle checkpoint. *Science*. 279:1045–1047.

King, R.W., R.J. Deshaies, J.-M. Peters, and M.W. Kirschner. 1996. How proteolysis drives the cell cycle. *Science*. 274:1652–1659.

Lengauer, C., K.W. Kinzler, and B. Vogelstein. 1997. Genetic instability in colorectal cancers. *Nature*. 386:623–627.

Li, X., and R.B. Nicklas. 1995. Mitotic forces control a cell-cycle checkpoint. *Nature*. 373:630–632.

Li, Y., and A.W. Murray. 1991. Feedback control of mitosis in budding yeast. *Cell*. 66:519–531.

Li, Y., and R. Benezra. 1996. Identification of a human mitotic checkpoint gene: hsMAD2. *Science*. 274:246–248.

Maddox, P.S., K.S. Bloom, and E.D. Salmon. 2000. The polarity and dynamics of microtubule assembly in the budding yeast *Saccharomyces cerevisiae*. *Nat. Cell Biol*. 2:36–41.

McEwen, B.F., A.B. Heagle, G.O. Cassels, K.F. Buttle, and C.L. Rieder. 1997. Kinetochore fiber maturation in PtK_1 cells and its implications for the mechanisms of chromosome congression and anaphase onset. *J. Cell Biol*. 137: 1567–1580.

Rieder, C.L, and R. Hard. 1990. Newt lung epithelial cells: cultivation, use, and advantages for biomedical research. *Int. Rev. Cytol*. 122:152–220.

Rieder, C.L., and E.D. Salmon. 1998. The vertebrate cell kinetochore and its roles during mitosis. *Trends Cell Biol*. 8:310–318.

Rieder, C.L., A. Schultz, R. Cole, and G. Sluder. 1994. Anaphase onset in vertebrate somatic cells is controlled by a checkpoint that monitors sister kinetochore attachment to the spindle. *J. Cell Biol*. 127:1301–1310.

Rieder, C.L., R.W. Cole, A. Khodjakov, and G. Sluder. 1995. The checkpoint delaying anaphase in response to chromosome monoorientation is mediated by an inhibitory signal produced by unattached kinetochores. *J. Cell Biol*. 130:941–948.

Roberts, R.T., K.A. Farr, and M.A. Hoyt. 1994. The *Saccharomyces cerevisiae* checkpoint gene BUB1 encodes a novel protein kinase. *Mol. Cell. Biol*. 14: 8282–8291.

Salmon, E.D., and P. Wadsworth. 1986. Applications of fluorescence in the biomedical sciences. Tayor, D.L., A.S. Waggoner, F. Lanni, R.F. Murphy, and R.R. Birge, editors. Alan R. Liss, New York. 639 pp.

Spurck, T.P., J.D. Pickett-Heaps, and M.W. Klymkowsky. 1986a. Metabolic inhibitors and mitosis. I. Effect of dinitrophenol/deoxyglucose on the live spindle. *Protoplasma*. 131:47–59.

Spurck, T.P., J.D. Pickett-Heaps, and M.W. Klymkowsky. 1986b. Metabolic inhibitors and mitosis: I. Effects of dinitrophenol/deoxyglucose and nocodazole on the live spindle. *Protoplasma*. 131:60–74.

Taylor, S.S., and F. McKeon. 1997. Kinetochore localization of murine Bub1 is required for normal mitotic timing and checkpoint response to unattached kinetochores. *Cell*. 89:727–735.

Thrower, D.A., M.A. Jordan, and L. Wilson. 1996. Modulation of CENP-E organization at kinetochores by spindle microtubule attachment. *Cell Motil. Cytoskel*. 35:121–133.

Visitin, R., S. Prinz, and A. Amon. 1997. CDC20 and CDH1: a family of substrate-specific activators of the APC-dependent proteolysis. *Science*. 278: 460–463.

Waters, J.C., T.J. Mitchison, C.L. Rieder, and E.D. Salmon. 1996. The kinetochore microtubule minus end disassembly associated with poleward flux produces a force that can do work. *Mol. Biol. Cell*. 7:1547–1558.

Waters, J.C., R.-H. Chen, A.W. Murray, and E.D. Salmon. 1998. Localization of Mad2 to kinetochores depends on microtubule attachment, not tension. *J. Cell Biol*. 141:1181–1191.

Waters J.C., R.-H. Chen, A.W. Murray, G.J. Gorbsky, E.D. Salmon, and R.B. Nicklas. 1999. Mad2 binding by phosphorylated kinetochores links error detection and checkpoint action in mitosis. *Curr. Biol*. 9:649–652.

Weiss, E., and M. Winey. 1996. The *S. cerevisiae* SPB duplication gene MPS1 is part of a mitotic checkpoint. *J. Cell Biol*. 132:111–123.

Zhang, D., and R.B. Nicklas. 1996. Anaphase and cytokinesis in the absence of chromosomes. *Nature*. 382:466–468.